



ELSEVIER

available at www.sciencedirect.com



journal homepage: www.elsevier.com/locate/jmbbm



Review article

Structure and mechanical properties of selected biological materials

P.-Y. Chen^a, A.Y.M. Lin^a, Y.-S. Lin^b, Y. Seki^a, A.G. Stokes^b, J. Peyras^a, E.A. Olevsky^c, M.A. Meyers^{a,b}, J. McKittrick^{a,b,*}

^a Materials Science and Engineering Program, UC San Diego, La Jolla, CA 92037-0411, United States

^b Department of Mechanical and Aerospace Engineering, UC San Diego, La Jolla, CA 92037-0411, United States

^c Department of Mechanical and Aerospace Engineering, San Diego State University, San Diego, CA 92182-1323, United States

ARTICLE INFO

Article history:

Received 7 November 2007

Received in revised form

1 February 2008

Accepted 2 February 2008

Published online 19 February 2008

Keywords:

Mechanical properties

Biological materials

Abalone

River clam

Sheep crab

Horseshoe crab

Antler

Hippo teeth

Warthog tusk

Great white shark teeth

Piranha teeth

Dogfish teeth

Toucan beak

Hornbill beak

ABSTRACT

Mineralized biological tissues offer insight into how nature has evolved these components to optimize multifunctional purposes. These mineral constituents are weak by themselves, but interact with the organic matrix to produce materials with unexpected mechanical properties. The hierarchical structure of these materials is at the crux of this enhancement. Microstructural features such as organized, layered organic/inorganic structures and the presence of porous and fibrous elements are common in many biological components. The organic and inorganic portions interact at the molecular and micro-levels synergistically to enhance the mechanical function. In this paper, we report on recent progress on studies of the abalone and Araguaia river clam shells, arthropod exoskeletons, antlers, tusks, teeth and bird beaks.

© 2008 Elsevier Ltd. All rights reserved.

* Corresponding author at: Department of Mechanical and Aerospace Engineering, UC San Diego, La Jolla, CA 92037-0411, United States.
Tel.: +1 (858) 534 5425; fax: +1 (858) 534 5698.

E-mail address: jmckittrick@ucsd.edu (J. McKittrick).

1. Introduction

The study of biological materials has received increasing interest in recent years due to the often extraordinary mechanical properties and unusual structures these materials possess. For example, the nacre of the abalone shell has been reported to have a work of fracture 3000 times over that of the mineral constituent (Jackson et al., 1988a). The compressive stress of a shark tooth bite is measured as high as 600 MPa (Snodgrass and Gilbert, 1967), even though this exceeds the compressive strength of the individual mineralized portions of the tooth (Craig and Peyton, 1958; Craig et al., 1961). Spider silk is reported to have a tensile strength similar to high-grade steel (Vollrath et al., 2001) and the gecko foot has been found to have exceptional adhesive strength based primarily on van der Waals forces (Autumn et al., 2000; Arzt et al., 2003). Biological structural materials fulfill numerous purposes. Antlers must flex without breaking and be impact resistant, mollusk shells must be able to sustain loads (wave and predator) without fracture, bones and teeth must maintain large compressive forces without buckling and/or cracking and plants must bend without tearing.

Many biological systems have mechanical properties that are far beyond those that can be achieved using the same synthetic materials (Vincent, 1991; Srinivasan et al., 1991). This is a surprising fact, if we consider that the basic polymers and minerals used in natural systems are quite weak. This limited strength of the components is the result of the ambient temperature, aqueous environment processing, as well as of the limited availability of elements (primarily C, N, Ca, H, O, Si). Biological organisms produce composites that are organized in terms of composition and structure, containing both inorganic and organic components in complex structures. They are hierarchically organized from the molecular to the macro (structural) level. The emerging field of the study of biological materials offers new opportunities to materials scientists to do what they do best: solve complex multidisciplinary scientific problems.

Hard biological materials are composites of an inorganic oxide phase with a biopolymer, created in a process called biominerization. Biominerized hydroxyapatite ($\text{Ca}_{10}(\text{PO}_4)_6(\text{OH})_2$, the main mineral component bone, teeth and antlers), calcium carbonate (CaCO_3 in the form of calcite or aragonite, the main component of seashells, bird eggs, crustaceans and coral) and amorphous silica ($\text{SiO}_2(\text{H}_2\text{O})_n$, the main mineral content of sponge spicules and diatoms) have been the primary materials examined.

The study of hard biological materials such as seashells, antler, teeth and bone have yielded fascinating insight into how these inorganic/organic materials adjust their microstructure and growth conditions to provide superior structural properties. A property map showing Young's modulus as a function of density is shown in Fig. 1. Biominerized composites such as the mollusk shell, coral, teeth, for example, are very lightweight but have a high elastic modulus. The densities of biological materials are generally less than 3 g/cm^3 . These materials have an integrated, hierarchical structure with an increasing complexity of the macroconstituents as the dimension becomes smaller. The macro shape has been optimized for external influences

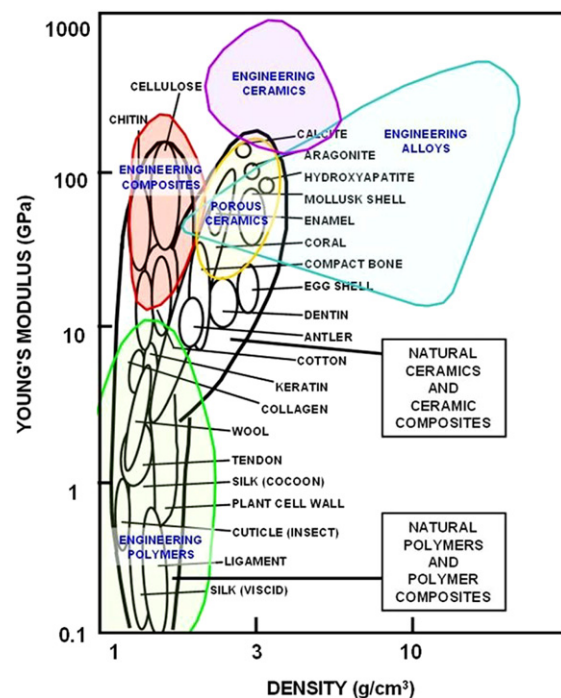


Fig. 1 – Young's modulus as a function of density for various biological materials, overlaid on a map indicating regions of synthetic materials (Adapted from Ashby (1989) and Wegst and Ashby (2004)).

such as protection and fighting and the nanoscale displays an intricate interaction between the mineral and organic components. This interaction, which has components of strong chemical and mechanical adherence, is maintained throughout the various length scales. It has been shown by Ji and Gao (2004) and Gao et al. (2003) that the scale of the components is important for the optimized performance. Using the Griffith criterion for brittle fracture, the stress (σ) required to activate a flaw of size $2a$ is:

$$\sigma = \frac{K_c}{\sqrt{\pi a}}$$

where K_c is the toughness of the brittle component. The fracture toughness is $\sim 1 \text{ MPa}\sqrt{\text{m}}$ for aragonite (Meyers et al., 2008a) and $\sim 1.2 \text{ MPa}\sqrt{\text{m}}$ for hydroxyapatite (van der Lang et al., 2002). From Fig. 1, the elastic modulus of aragonite and hydroxyapatite is $\sim 100 \text{ GPa}$. Estimating that the theoretical strength of the material is $E/10$, this strength is reached for $\sim 25 \text{ nm}$. This is part of the reason why the brittle component scale is in the nanometer range.

One striking similarity between mineralized tissues of various taxa is the presence of organized layered structures of soft and hard material. The mineralized phase provides strengthening and the organic phase provides toughness. This is observed in seashells and, to some extent, in compact bone. The interaction of the mineralized and organic components produces a synergistic effect that enhances mechanical properties. Another similarity is the presence of porous (foam) material in taxa that are ambulatory, as displayed in bones, antlers, arthropod exoskeletons, teeth and bird beaks. The porous material provides a lightweight

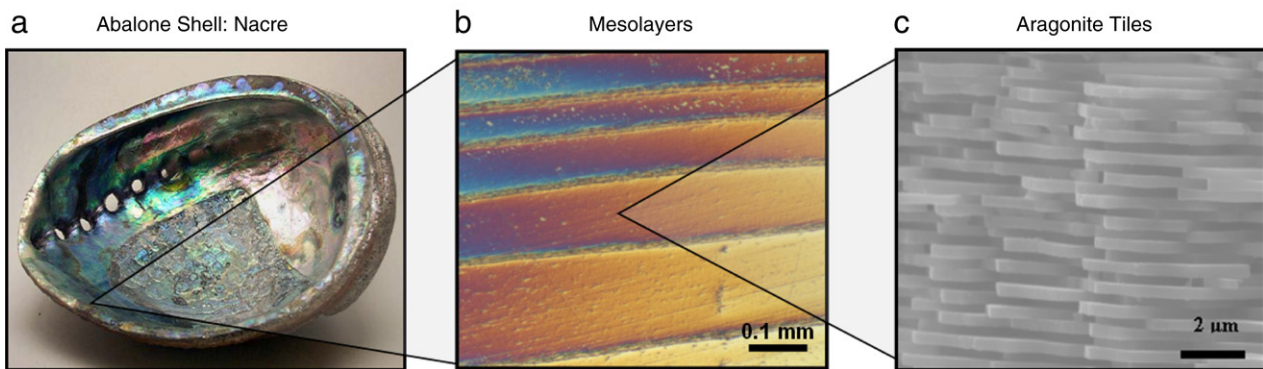


Fig. 2 – Hierarchical structure of abalone shell. (a) Macro-, (b) meso- and (c) micro-scale.

framework and increases the stiffness of the biological component. Fibers are also preponderant in biological materials. Bones, teeth, arthropod exoskeletons and antler all have some fibrous component. Anisotropy of the fibers plays a major role in determining the mechanical properties of these components.

Analysis of laminates, porous and fibrous structures are at the heart of understanding the mechanical properties of biological materials. In this paper, we report recent progress on the structure and mechanical properties of the abalone and river clam shells, crab exoskeletons, antler, teeth, tusks and bird beaks.

1.1. Abalone shell

The abalone shell (*Haliotis rufescens*) has two layers: an outer prismatic layer (rhombohedral calcite) and an inner nacreous layer (orthorhombic aragonite) as observed by Nakahara et al. (1982). Fig. 2(a) shows a shell with its nacreous (internal) surface exposed. The nacreous portion is composed of mesolayers of ~0.3 mm thick, separated by organic layers embedded with calcium carbonate (Meyers et al., 2008a,b).

These mesolayers are thought to be the result of growth bands and are visible in the optical micrograph of Fig. 2(b). Aragonitic CaCO_3 constitutes the inorganic component of the nacreous ceramic/organic composite (95 wt-% ceramic, 5 wt-% organic material). This composite is comprised of stacked platelets (~0.5 μm thick), arranged in a ‘brick-and-mortar’ microstructure with an organic matrix (20–50 nm thick) interlayer that is traditionally considered as serving as glue between the single platelets (Fig. 2(c)). As a result of this highly ordered hierarchical structure nacre exhibits excellent mechanical properties. Details of the structure and growth can be found in our work (Menig et al., 2000; Lin and Meyers, 2005; Lin et al., 2006, 2007; Meyers et al., 2008b) and others (Watanabe and Wilber, 1960; Wada, 1964; Towe and Hamilton, 1968; Bevelander and Nakahara, 1970; Erben, 1972; Sarikaya and Aksay, 1992; Fritz et al., 1994; Manne et al., 1994; Falini et al., 1996; Zaremba et al., 1996; Schäffer et al., 1997; Addadi et al., 2006).

Fig. 3 summarizes the strength of nacre with respect to various loading directions. The unique strength anisotropy perpendicular to the layers (5 MPa vs. 540 MPa) is remarkable (Jackson et al., 1988b; Meyers et al., 2008a,b). Another marked

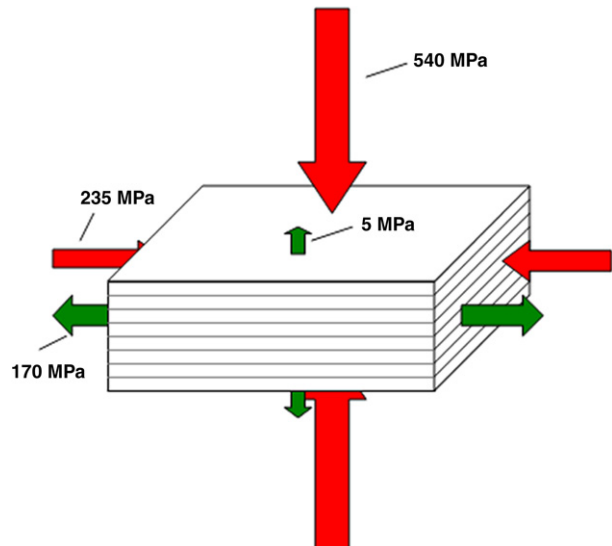


Fig. 3 – Compressive and ultimate tensile strengths of nacre under different to loading direction.

characteristic is the greater compressive strength when loading is applied perpendicular rather than parallel to the tiles. This is due to the phenomena of axial splitting and microbuckling (kinking) when loading is applied parallel to the tiles. The relatively small difference in tensile and compressive strength (170 MPa vs. 230 MPa (Menig et al., 2000)) in this direction of loading is directly related to the high toughness, possibly attributed to the existence of inter-tile mineral bridges in combination to the organic “glue”. These mineral bridges exist as the continuation of a single crystal between consecutive layers of aragonite tiles.

Fig. 4 is a schematic showing the failure mechanisms for the different load applications and directions. Compression perpendicular to the surface of the shell yields the highest value, and failure occurs in an axial splitting mode. Compression parallel to the shell surface, on the other hand, reveals a fracture mode akin to plastic microbuckling (not always, but on a significant fraction of cases). This has been analyzed in detail by Menig et al. (2000). Failure in tension when the loading direction is parallel to the shell surface occurs by sliding of the tiles, so that this is relatively

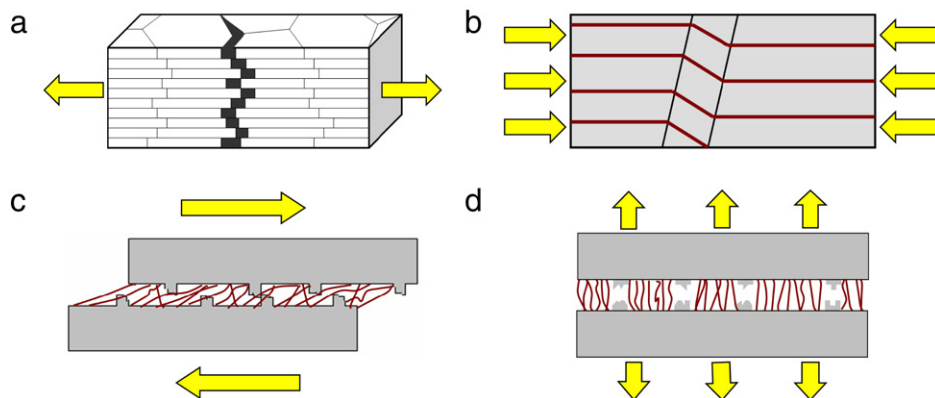


Fig. 4 – Failure mechanisms of abalone shells in different loading conditions: (a) Tension parallel to shell surface (b) compression parallel to shell surface (c) shear parallel to shell surface (d) tension perpendicular to shell surface.

brittle fracture. Thus, the shear strength of the organic inter-tile layer is about the same (or higher) than the tensile strength of the tiles, and failure occurs by inter-tile shear. For tensile loading perpendicular to the shell surface, the primary mechanisms seem to be fracture of the inter-tile bridges and extension of the organic layer gluing the adjacent layers.

Inter-tile mineral artifacts have been observed through transmission electron microscopy (TEM) as can be seen in Fig. 5. To prove that a mineral connection exists, selected area diffraction patterns were obtained for consecutive layers of tiles. Tiles in a stack showed identical crystal orientation, indicating single crystal continuity only possible through a mineral connection. These have been presented in Fig. 6(a) and (b) and are in agreement with results by Feng et al. (1999) who also showed high degree of crystallographic texture characterized by a nearly perfect “c-axis” alignment normal to the plane of the tiles through selected area diffraction patterns. The observed mineral bridges are believed to grow as consecutive layers of tiles are formed and mediated through a series of porous organic membranes. This has been well described by Cartwright and Checa (2007). Recent findings suggest that they play a critical role in both the growth and the mechanical strengthening of the composite (Lin et al., 2007; Meyers et al., 2008b). The organic matrix was once thought to provide the primary interfacial toughening mechanisms. By observing the large ratio of compressive to tensile strength when loading is perpendicular to the tiles (Fig. 3), one can begin to estimate the tensile strength of an individual mineral bridge (Meyers et al., 2008b). Although there are a high number of bridges per tile (a density of approximately $2.25/\mu\text{m}^2$ per tile), the total area along which a load can be applied in tension is still a fraction of the composite area. Thus a relatively low strength (5 MPa) is observed in this loading direction. Song et al. (2002) were among the first to identify these bridges and to estimate quantitatively their number. Barthelet et al. (2006) and Meyers et al. (2008b) confirmed their presence.

1.2. Araguaia river clam

The Araguaia river clam is found to exist in fresh water of the Amazon basin. In its natural environment it sits upright

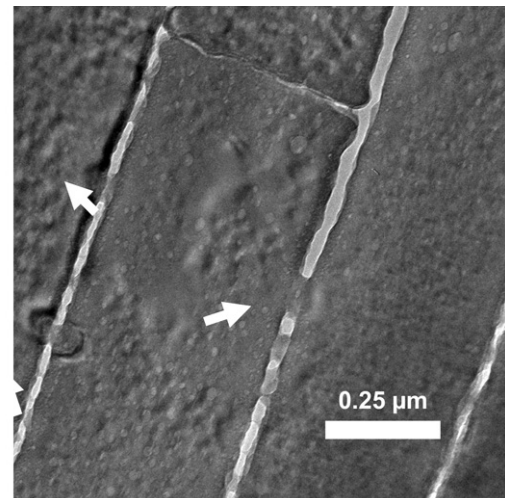


Fig. 5 – Transmission electron micrograph of nacre crosssection showing mineral bridges between tile interfaces.

with its flat bottom base seated in the floor of a sandy river bed. Protruding, upward its shell makes a fin-like arc (Fig. 7(a)) cutting through the current of the moving river, allowing the capture of passing food. Although the environment of this freshwater bivalve differs greatly from that of the red abalone, their structures both consist of aragonite tiles. However, there are significant differences in this structure and, thus, differences in their mechanical response.

The shell of the Araguaia river clam consists of parallel layers of calcium carbonate tiles, approximately $1.5 \mu\text{m}$ in thickness and $10 \mu\text{m}$ in length. This is three times thicker, and twice the length of the previously studied abalone nacre, implying a higher inorganic to organic ratio. Furthermore the uniformity of the tiles is far less apparent in the shell of the river clam than the abalone. Although a uniaxial alignment is observed along the c-axis (the axis parallel to the direction of growth) the consistency of layer thickness is less pronounced than its saltwater counter part. The wavy structure is observed in Fig. 7(c) and can be seen throughout.

The greatest difference between the two structures, however, is at the macrolevel. In contrast to the abalone shell,

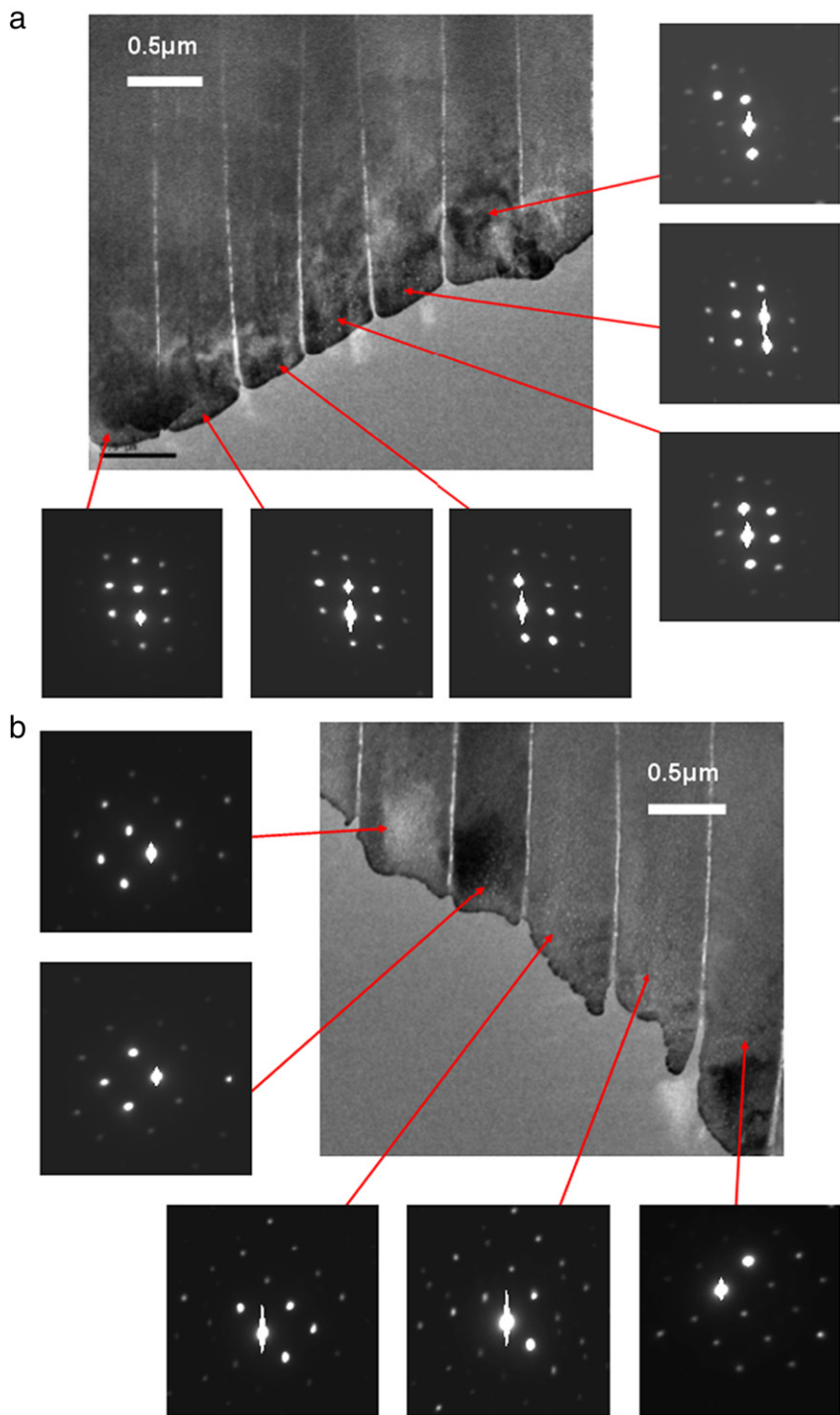


Fig. 6 – Two samples of abalone nacre (a) and (b) characterized through transmission electron microscopy. Consistent crystal orientation is observed through selected area diffraction of consecutive layers of aragonite tiles indicating a single crystal structure through several layers.

there were no observed mesolayers marking inorganic growth interruption. Fig. 7(b) provides an optical view of the cross-section of the river clam shell. The missing growth bands and decreased organic composition lead to a more classically brittle ceramic. While mechanisms such as crack deflection and microbuckling were observed in the abalone nacre (Menig et al., 2000) they were lacking in the river clam shell. Fig. 8(a)

shows the unobstructed crack propagation in the river clam shell. In some places, plate pull-out was observed (Fig. 8(b)), but this was not the most common response.

Three-point bending and quasi-static compression tests were conducted in various orientations of shell microstructure. Compression sample were cut into cubes of approximately 5 mm. Load directions perpendicular and parallel to

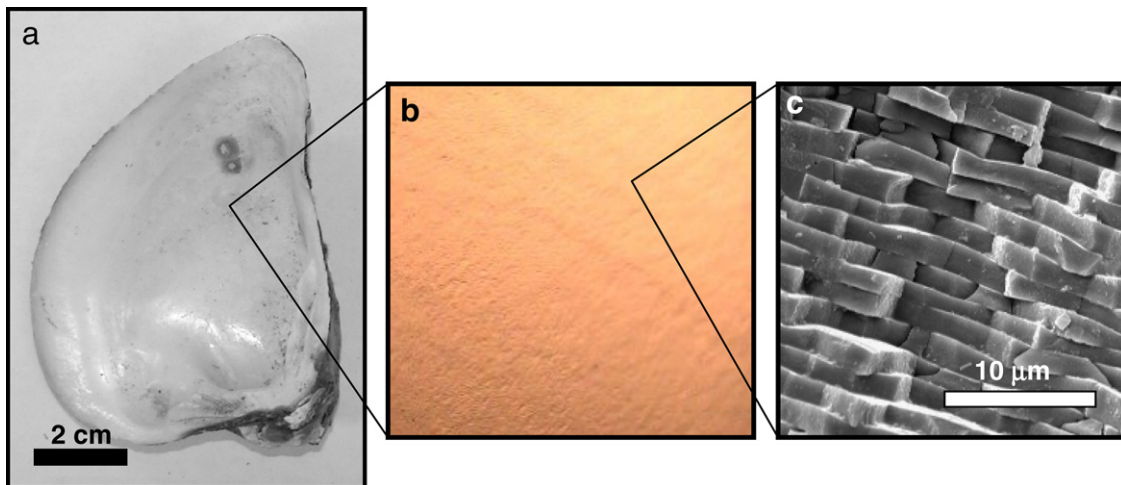


Fig. 7 – Structural hierarchy of the Araguaia river clam. (a) Note flat bottom which ensures that the clam stays upright on the sandy river bed. (b) There is little or no observable mesolayers at the mesoscale. (c) Thick wavy tiles of 1.5–2 μm in thickness and 10 μm in length are observable at the microscale.

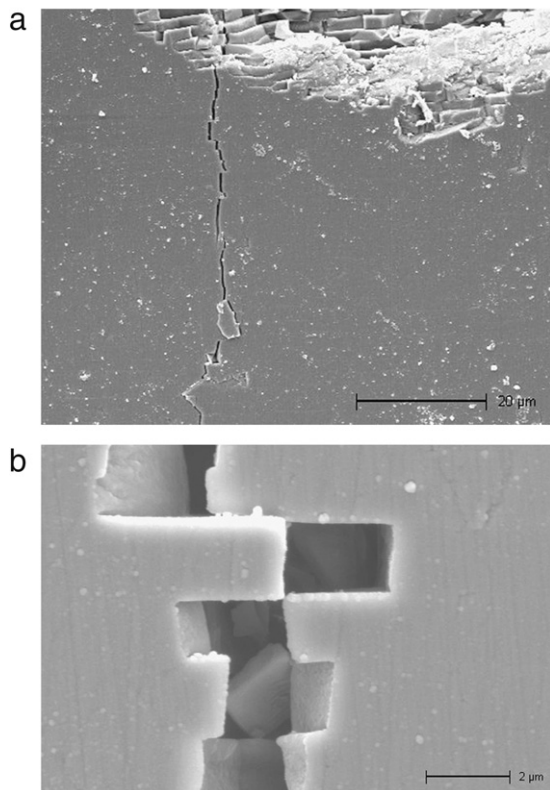


Fig. 8 – Crack propagation in fractured Araguaia river clam shell; (a) through-tile fracture; (b) region with tile pull-out.

growth layers are represented in Fig. 9(a). Bending (flexure) samples were prepared to an approximate length to thickness ratio of 8:1, with square cross sections of roughly 4 mm thickness. The average length of each samples was 30 mm.

As in all biological samples, the wide variation in results requires a statistical analysis. Therefore, the Weibull analysis was applied and represented in Fig. 10. The material shows a strong dependence of orientation in failure strength. The

compressive strength when loaded perpendicular to the layers is 40% higher than when it is loaded parallel to them. The 50% fracture probability is found at 567 MPa for the perpendicular direction and 347 MPa for the parallel (Fig. 10(a) and (b)). This compressive strength is roughly 20–35 times greater than flexural strength of 15 MPa observed in both directions of loading (Fig. 10(c) and (d)). This ratio of compressive to flexural strength is far greater than what is found in abalone nacre, and represents a brittle ceramic. This may be attributed to the lack of the macroscaled organic laminate mesolayers.

1.3. Arthropod exoskeletons

The arthropod exoskeleton is a natural composite which is multifunctional, hierarchically structured, and highly anisotropic in mechanical properties. Exoskeletons from two species, sheep crab (*Loxorhynchus grandis*) and horseshoe crab (*Limulus polyphemus*), have been investigated by our group. The arthropod exoskeleton is multifunctional: it supports the body, resists mechanical loads, and provides environmental protection (Vincent, 1991, 2002). The exoskeleton comprises three main layers, epicuticle, exocuticle, and endocuticle. The outermost epicuticle is a thin waxy layer, which acts as waterproofing barrier. Beneath the epicuticle is the exocuticle (outer) and endocuticle (inner), the main structural component, which is primarily designed to resist mechanical loads. There is a high density of pore canals containing tubules penetrating through the exoskeleton in the direction normal to the surface. These tubules play an important role in the transport of mineral ions and nutrition during the formation of the new exoskeleton after the molting.

The arthropod exoskeleton consists mainly of chitin and protein. In crustaceans (e.g. crabs and lobsters), there is a high degree of mineralization, typically CaCO_3 in the form of calcite. Fig. 11(a) shows the hierarchical structure of a sheep crab (*L. grandis*) exoskeleton. At the molecular level, chitin chains form fibrils of 3 nm in diameter and

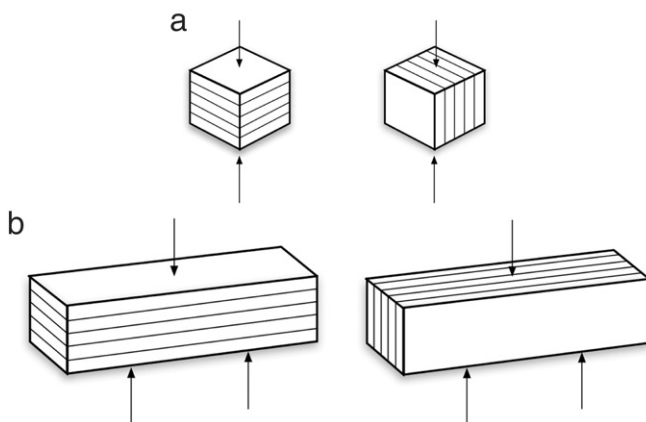


Fig. 9 – (a) Quasi-static compression testing geometry. Compression direction perpendicular to layers on the left, and parallel on the right. (b) Three-point bending geometry. Load direction perpendicular to layers left, and parallel right.

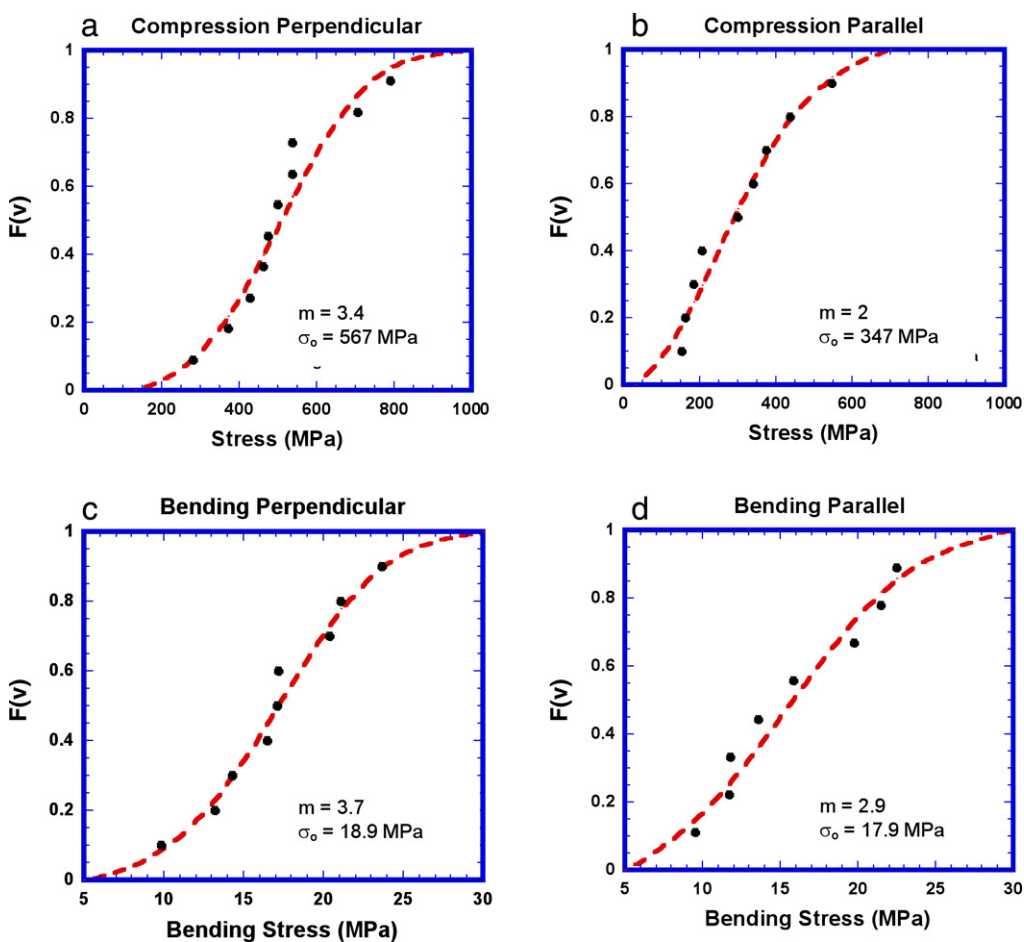


Fig. 10 – Strength (Weibull) distribution for Araguaia river clam: (a) compression perpendicular to layered structure; (b) compression parallel to layered structure; (c) three-point bending perpendicular to layered structure; (d) three-point bending parallel to layered structure. m = Weibull modulus, σ_0 = characteristic strength.

300 nm in length. The fibrils are wrapped with proteins and assemble into fibers of about 60 nm in diameter. These fibers further assemble into bundles. The bundles form horizontal planes stacked in a helicoidal fashion, creating

a twisted plywood structure. A complete 180° rotation is referred to as a Bouligand layer (Bouligand, 1972; Giraud-Guille, 1984). The Bouligand layer corresponds to the layers in exocuticle and endocuticle. Fig. 11(b) shows the hierarchical

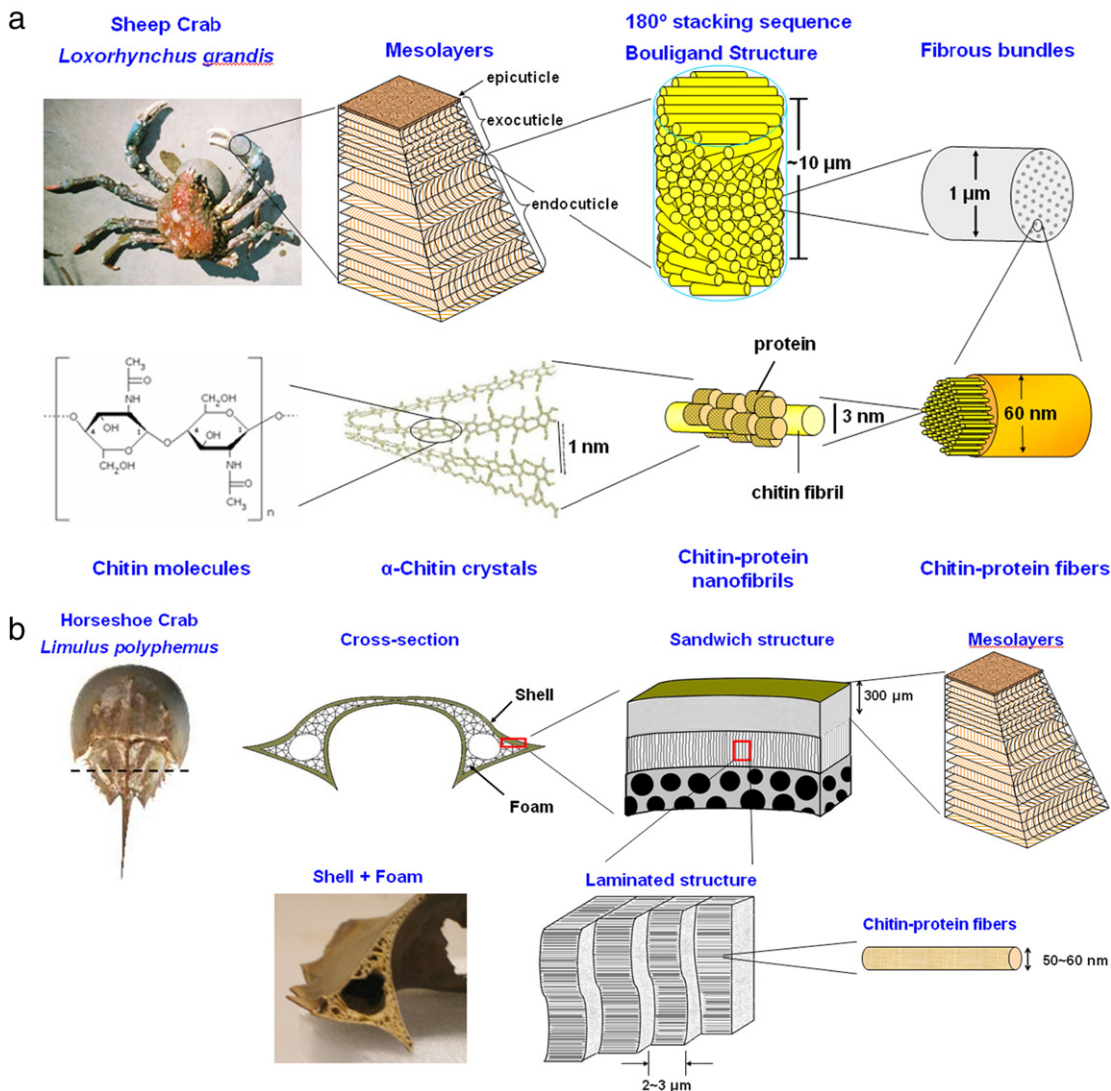


Fig. 11 – Hierarchical structure of (a) sheep crab (*Loxorhynchus grandis*), and (b) horseshoe crab (*Limulus polyphemus*) exoskeletons.

structure of horseshoe crab (*Limulus polyphemus*) exoskeleton. The horseshoe crab is a living fossil, which has existed for more than 200 million years. Horseshoe crabs are genetically more similar to scorpions and spiders than to other crabs. The exoskeleton of horseshoe crabs is a sandwich composite consisting of three layers: an exterior shell, an intermediate layer, and an interior core. The exterior shell of horseshoe crab is similar to crab exoskeletons with no mineral presence. Beneath the exterior shell is an intermediate layer consisting of vertical laminate about $2\text{--}3 \mu\text{m}$ wide that connects the exterior shell to the interior core. The interior core has an open-cell foam structure and is hollow in the middle. The cellular network is akin to the interior structure of toucan and hornbill beaks, as described in the below section. Fig. 12(a) is a scanning electron microscope (SEM) micrograph showing the Bouligand structure (brace) of sheep crab exoskeleton. In the normal direction, there are ribbon-like tubules (arrows) going through the layers. The width of a single tubule is about $1 \mu\text{m}$ and the thickness is about $0.2 \mu\text{m}$. Fig. 12(b) shows the exterior shell and intermediate layer of the horseshoe crab

exoskeleton. The exterior shell has layered structure, which is akin to crab exoskeletons consisting epicuticle, exocuticle, and endocuticle. The intermediate layer is composed of vertically oriented laminate \sim 2–3 μm thick.

The mechanical properties of arthropod exoskeleton are highly anisotropic. Tensile tests were performed on sheep crab exoskeletons in two different directions: longitudinal direction (y -direction) and direction normal to the surface (z -direction) (Chen et al., 2008). For the walking legs, in the y -direction, the stress-strain curve is linear and fracture occurs at 12.5 ± 2.3 MPa and $1.7 \pm 0.3\%$ strain. The flat fracture surface corresponds to brittle failure. In the z -direction, a non-linear plastic deformation is observed and the ultimate tensile strength reaches 18.8 ± 1.5 MPa and $4.7 \pm 1.2\%$ strain. There is a high density of tubules ruptured in tension and necking can be observed. Tubules act as the ductile component that helps to stitch the brittle bundles arranged in Bouligand pattern and enhance toughness.

Hardness tests were conducted on the claw and walking leg of sheep crab from the surface through the thickness

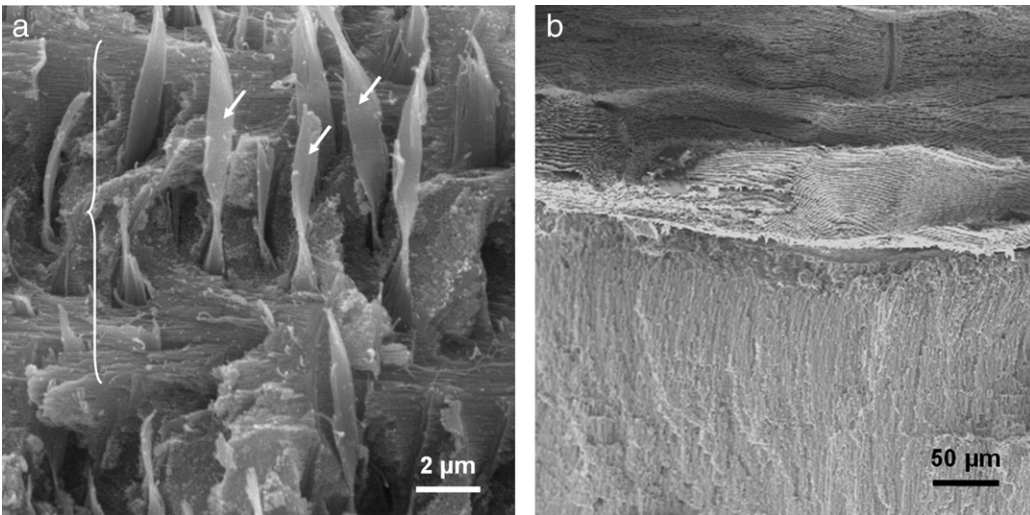


Fig. 12 – SEM micrographs showing (a) the Bouligand structure of the sheep crab exoskeleton. (Brace: 180° rotation of Bouligand structure. Arrows: ribbon-shaped pore canal tubules) (b) the external shell and intermediate laminated layers of horseshoe crab exoskeletons.

of exoskeleton. The results show that the exocuticle is much harder than endocuticle. A discontinuity of hardness values across the interface between the exocuticle and the endocuticle is observed. The hardness values are 948 ± 108 MPa (claw) and 238 ± 35 MPa (walking leg) in the exocuticle region (~ 200 μm thick) and drop to a much lower value, ranging 440 – 540 MPa (claw) and 130 – 142 MPa (walking leg) in the endocuticle (~ 2.5 mm thick). This is due to the higher mineral content and the more densely packed structure in the exocuticle. The hardness values of the claw are about 3–4 times higher than those of the walking legs. This correlates with the higher mineral content in claw (78.5 wt% ash) compared to the walking leg (63.5 wt% ash). The hardness values measured in this work are higher than those of the American lobster claw (130–270 MPa in exocuticle and 30–55 MPa in endocuticle) (Raabe et al., 2005). This may also relate to the higher mineral content in sheep crab compared with the American lobster, which has an ash content of $63.6 \pm 4.3\%$ of dry weight. Such design (hard, thin layer on the surface) is widely used in nature. For example, teeth and tusks are comprised of a hard external hard enamel and internal tough dentine.

1.4. Antlers

Antlers offer an interesting area of study because they are one of the most impact resistant and energy absorbent of all biominerized materials. Antlers are bony protuberances that form on the heads of animals from the Cervidae family (deer). The Cervidae family includes deer, moose, North American elk (wapiti) and reindeer (caribou). Antlers are one of the fastest growing organs in the animal kingdom, growing as much as 14 kg in 6 month, with a peak growth rate of up to 2–4 cm/day (Goss, 1983). The antler is the only mammalian bone that is capable of regeneration, offering unique insight into bone growth. Antlers are deciduous and are cast off (dropped) at the end of the rut (Sept.–Nov.). Antlers have two primary functions: they serve as visual signs of social

rank within bachelor groups (Geist, 1966; Henshaw, 1971; Lincoln, 1972; Clutton-Brock, 1982) and are used in combat, both as a shield and as a weapon (Geist, 1966). During the rut, male deer fight for control of harems, which involves charging, butting heads and interlocking antlers. The antlers have been designed to undergo high impact loading and large bending moments without fracture. The unusual strength of antlers is attested by the very few observations of antler breakage during fighting in large groups of caribou and moose (Henshaw, 1971).

Antlers have a composition and structure similar to other mammalian long bones, but there are distinct differences. Bones are load bearing and contain essential interior fluids (blood, marrow, etc.). Bones produce vital cells necessary for the body whereas antlers remove fluids and minerals from the body in order to grow. Antler growth (antlerogenesis) necessitates a large amount of calcium and phosphorus in a short period of time. Red deer (*Cervus elaphus*, a European deer almost identical to the North American elk) antlers require ~ 100 g/day of bone material in comparison to the growing fawn skeleton that take ~ 34 g/day (Chapman, 1975). This quantity of minerals cannot be obtained through food sources alone and has been shown to originate from the skeleton of the animal (Meister, 1956; Chapman, 1975; Goss, 1983; Muir et al., 1987; Harvey and Bradbury, 1991). The long bones of the legs and the ribs are the richest source of these minerals, and these bones are found to decrease in density as the antlers increase in size. Bone resorption occurs alongside bone remodeling during antlerogenesis. Another difference between antlers and other bones is the mineral content. Antlers have ~ 50 wt% mineral content whereas bones are between 60–70 wt% (Currey, 1979).

Fig. 13 shows the hierarchical structure of antlers. Antlers contain a core of trabecular (cancellous) bone surrounded by compact bone that runs longitudinally through the main beam of the antler and the prongs. The trabecular bone is anisotropic, with somewhat aligned channels directed parallel to the long axis of the antler beam. Compact

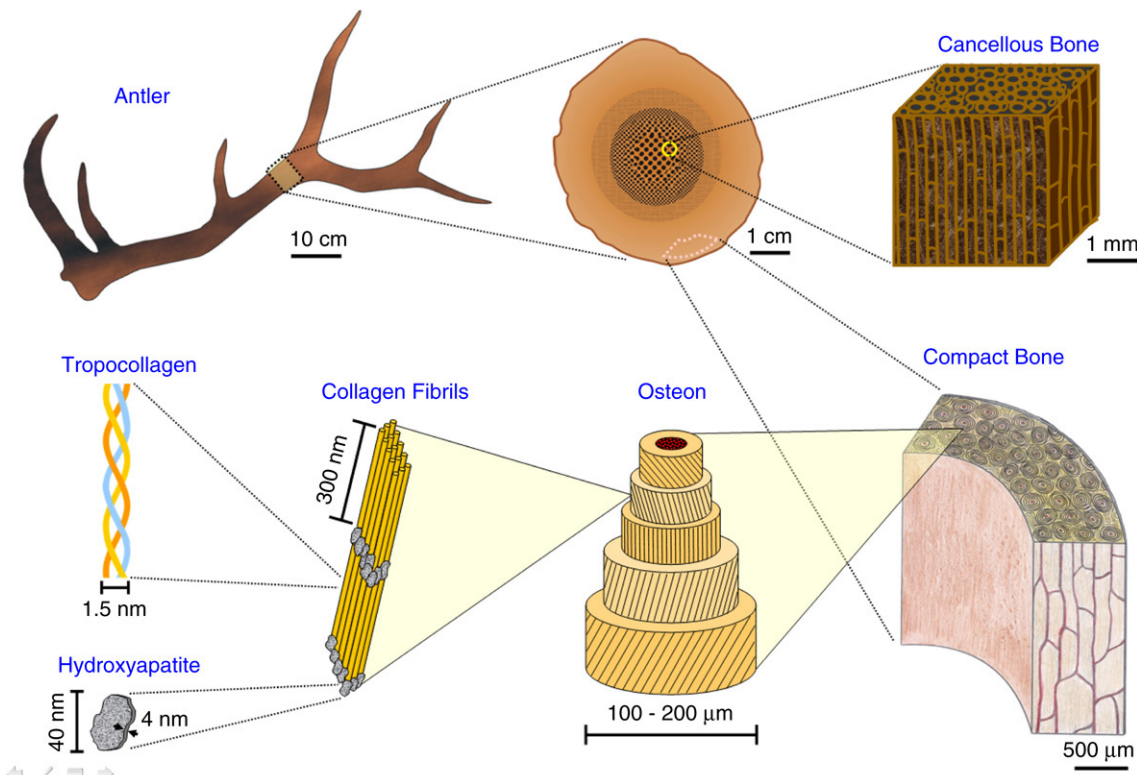


Fig. 13 – Hierarchical structure of antlers. Antlers are composed of primarily compact bone as the outer layer and trabecular (cancellous or spongy) bone in the interior. The compact bone consists of osteons, which supply blood to the growing antler through the vascular channels in the osteons.

bone surrounds this core, consisting of osteons that have a laminated structure of concentric rings extending from the main channel (blood vessel). The concentric rings contain aligned collagen fibrils that have the mineral, hydroxyapatite, dispersed on or between the fibrils. The alignment of the collagen fibrils changes direction between the laminates.

The antlers from the North American elk (*Cervus canadensis*) were examined in this study. Fig. 14(a) shows a photograph of a cross-section of piece taken from the long beam of the antler. The thin, outer most layer is the subvelvet zone, below which is the compact bone. There is a transition region between compact bone and the porous, spongy bone (trabecular bone) in the interior (Currey, 1988). This is to be contrasted with the long bones of mammals, which have a hollow interior (except at the head of the bone, where cancellous bone is found). The inset shows the osteons in the compact bone, which has the same configuration of other mammalian bones. Fig. 14(b) shows a computer tomography (CT) scan of the longitudinal cross-section demineralized portion of the antler. The elongated channels in the trabecular bone can be seen.

Some mechanical testing has been performed on antlers. Currey first performed experiments on bones and antlers taken from various species (Currey, 1979, 1988, 1989, 1990) and found that the elastic modulus increased and toughness decreased with increasing mineral content. Blob et al. tested white tailed deer (Blob and LaBarbera, 2001) (*Odocoileus virginianus*) and moose (*Alces alces*) (Blob and Snelgrove, 2006) antlers and found no correlation of the elastic modulus

as a function of the position along the antler, suggesting that other mechanical properties may not be influenced by the location. Moose antlers had a higher elastic modulus (11.6 GPa) compared to the white-tailed deer (6.8 GPa). The difference was attributed to the different fighting behavior between moose and the white-tailed deer as a consequence (or a predator) of the different antler structure. Moose have large palmate antlers, with small prongs surrounding it. Deer have a long antler beam with prongs extending from this central beam. As a consequence, fighting moose cannot interlock their antlers and are thus subjected to higher bending moments. The elastic modulus of the elk antler is ~7.5 GPa, which is smaller than for moose and larger than for white-tailed deer. As expected, it is nearly identical to that of red deer (7.4 GPa, (Currey, 1979)).

Fig. 15 shows a Weibull plot of the dry tensile strength in the longitudinal and transverse direction of compact bone along the main beam of the elk. The plot shows that the strengths can be fit with Weibull statistics. The strength in the transverse direction ($N = 9$) has an average failure strength of 20.3 ± 6.0 MPa compared with the longitudinal strength of 115.4 ± 16.6 MPa ($N = 7$). The strength in the longitudinal direction is lower than the antler strength of the spotted deer (*Axis axis*) of 188 ± 12 MPa (Rajaram and Ramanathan, 1982), and the red deer (158 MPa) and larger than reindeer (*Rangifer tarandus*, 95 MPa) (Currey, 1990). For comparison, the dry longitudinal tensile strength of the compact bone of a cow femur is 148 MPa (Currey, 1990). These comparable values indicate the similarity of structure of compact bone

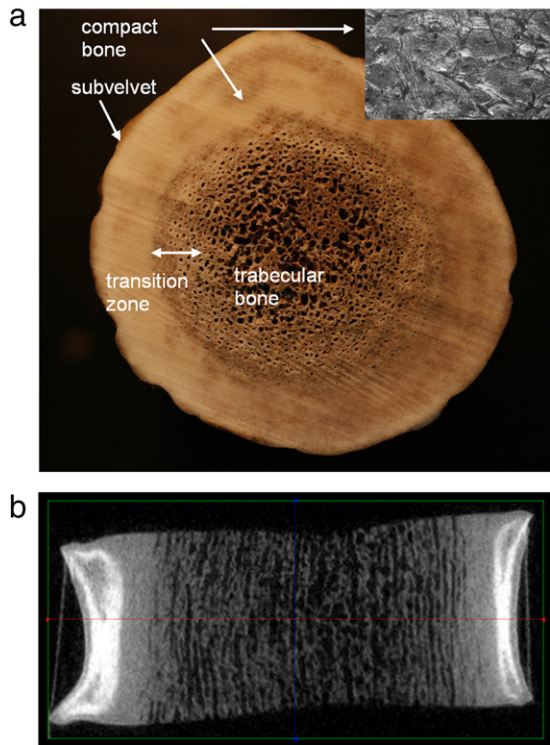
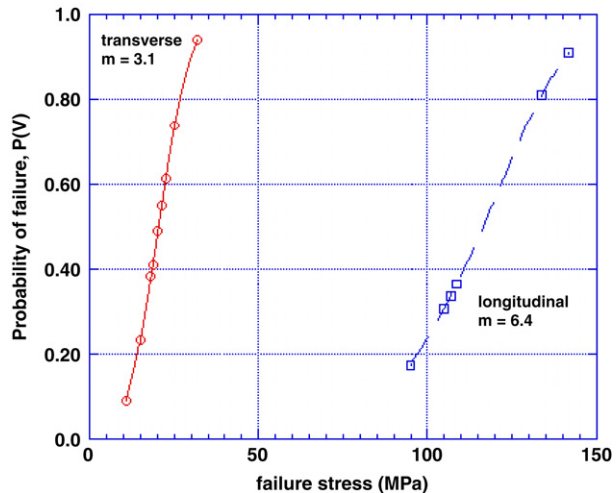


Fig. 14 – (a) Cross-section through the main beam of an elk antler. The thin outer surface is the subvelvet zone followed by compact and trabecular bone. A transition zone separates the compact and trabecular regions. Inset is an SEM micrograph of the compact bone showing the osteons. **(b)** Computer tomography scan of a demineralized antler.

in long bones and in antlers. The Weibull modulus in the transverse direction is smaller than in the longitudinal direction, illustrating larger scatter in the data. This is a consequence of the anisotropic orientation of mineralized collagen fibers. The collagen fibers are oriented roughly along the longitudinal axis, preventing cracks from propagating. In the transverse direction, cracks can more easily propagate through the interstices between neighboring lamellae and the value of tensile strength in the transverse direction depends on the presence of surface cracks.

1.5. Tusks and teeth

Teeth are the most mineralized component of vertebrate animals and are composed of four parts. The outer layer is enamel, with a mineral content of 96% hydroxyapatite in the form of woven rods. Below the enamel is dentin containing 30% type-I collagen, 25% fluid and 45% nanocrystalline carbonated apatite (Imbeni et al., 2003; Meyers et al., 2008a). Cementum, covering the root of the tooth, has ~65% hydroxyapatite, 23% type-I collagen and 12% water. Finally, dental pulp is at the center of the tooth is highly vascularized with nerves, cells and some type-I collagen. Depending on the diet of the animal, teeth are optimized for chewing (herbivores) or biting and tearing (carnivores). A tusk is an extremely long mammalian tooth that protrudes from the



**Fig. 15 – Weibull plot of the dry transverse and longitudinal strengths of the elk antler.
m = Weibull modulus.**

mouth. Tusk-bearing mammals include the walrus, elephant, warthog and narwhal. Large teeth and tusks are often used interchangeably to describe ivory.

Hippopotamus (*Hippopotamus amphibius*) have very large curved canines in front, slightly smaller incisors just behind the canines and molars in the back. The molars and incisors are used for chewing and it is speculated that once the molars lose their grinding effect due to wear the hippopotamus dies (Laws, 1968). The canines appear to be used for defensive purposes and fighting for dominance. A photograph of a canine hippo tooth is shown in Fig. 16(a). The tooth is curved and has a length of ~10 cm. A typical cross-section of the tooth is shown in Fig. 16(b) (Espinoza and Mann, 1991). The structure is similar to other mammalian teeth, with dentin as the largest fraction surrounded by a thin layer or enamel or cementum. The interstitial zone is also known as the pulp cavity. The enamel of the hippo tooth has a density of 1.7 g/cm³, had a compressive elastic modulus (enamel and dentin) of ~2.6 GPa and a hardness of 1.7 GPa for enamel and 0.3 GPa for dentin. This compares favorably with human teeth with a hardness of 3.2–4.4 GPa for enamel and 0.25–0.80 GPa for dentin (Marshall et al., 1997). The dentine-enamel interface has been shown to be an effective crack arrester. Cracks starting in the harder enamel are arrested at the interface (Imbeni et al., 2005).

Warthogs (*Phacochoerus Africa*) have two pairs of tusks on the lower and upper jaw. The tusks are the canine teeth, which continue growing during the life of the animal. The upper canines grow from 20–50 cm, while the lower ones grow to about 10 cm. The upper tusks (Fig. 16(b)) grow out and curve up around the snout and are relatively dull. The lower tusks are short and straight and are used for defense and are kept self-sharpened due to rubbing against the upper tusks. The tusks are sometimes used for digging but are generally used for fighting with other warthogs and for fending off predators. Fighting between warthogs for mating rights is usually done with a closed mouth where the warthogs face head to head and shove each other with the help of the dull upper tusks. On

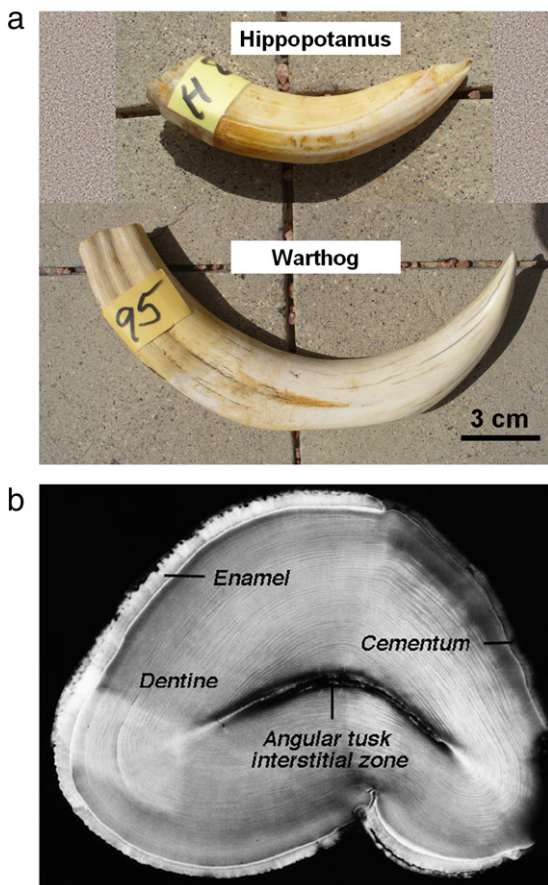


Fig. 16 – (a) Photograph of the hippopotamus canine tooth and warthog tusk, **(b)** cross-section of the hippo tooth (Espinoza and Mann, 1991).

the other hand, warthogs will use their sharp lower tusks and an open mouth causing considerably more damage to fend off predators. Fig. 17 shows an SEM micrograph of a fracture surface of the dentin in the warthog tusk. The channels observed are the dentin tubules, which extend both from the enamel-dentin and cementum-dentin. The tubules contain fluid and cells and are surrounded by a highly mineralized layer and are oriented perpendicular to the collagen fibrils in the dentin (Marshall et al., 1997). The tubule diameter ($\sim 1.3 \mu\text{m}$) is on the order of what is reported for human dentin ($\sim 1.8 \mu\text{m}$) (Marshall et al., 1997) and observed in elephant tusks ($\sim 1 \mu\text{m}$) (Nalla et al., 2003). There was great variability in the tensile strength of the tusk in the longitudinal direction, ranging between 12–45 MPa. This variability is most likely due to the difficulty in obtaining reliable test specimens from the curved tusk.

One particularly important aspect of canine teeth is that the animal has the ability to sharpen their tip throughout its life. This has an obvious advantage for effective defense and hunting skills. This is accomplished in rodents and boars, and Fig. 18 illustrates this effect. Fig. 18(a) shows the incisor teeth in a rat. During eating, the dentin is eroded and results in a sharp enamel edge being continuously exposed. This must be done continuously as these teeth keep growing during the life of the animal. Boars use the same approach to ensure

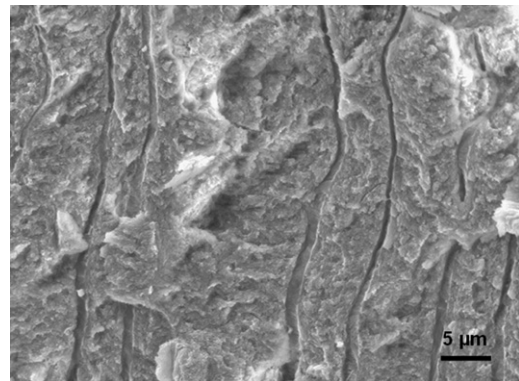


Fig. 17 – SEM micrograph of a fracture surface of a warthog tusk. The channels are the dentin tubules, which is surrounded by a collagen/mineral matrix.

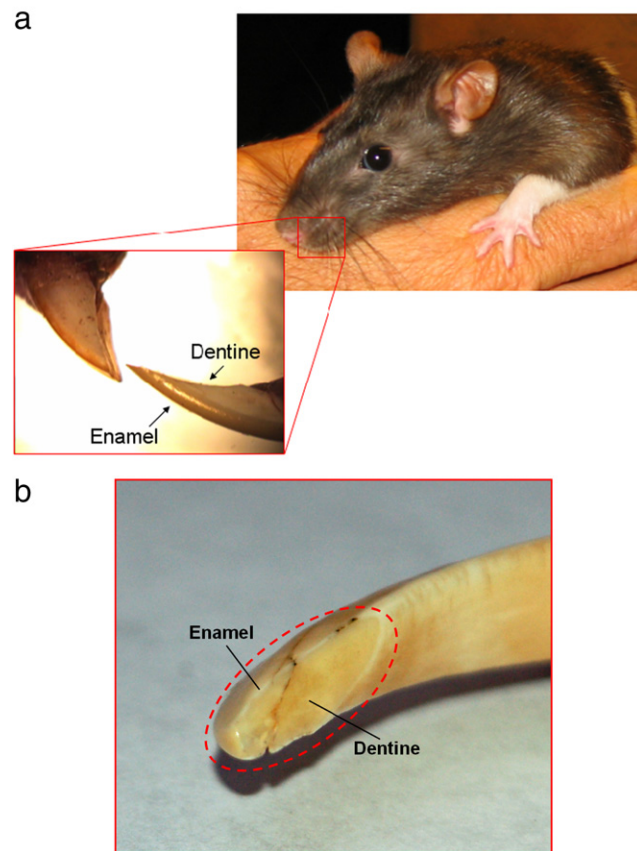


Fig. 18 – (a) Incisor from a rat showing both the enamel and the dentine; **(b)** tusk in boar showing wear of dentine at tip, ensuring a sharp enamel edge.

a lethal cutting edge in the lower tusks. The area where wear is observed is marked in Fig. 18(b), indicating this self-sharpening mechanism.

The Amazon dogfish (*Rhaphiodon vulpinus*) is a freshwater fish found in Central and South American river basins. It has two long teeth that penetrate through the mouth, as shown in Fig. 19. As shown in the SEM micrograph, the teeth are microstructurally smooth. The main function of these teeth

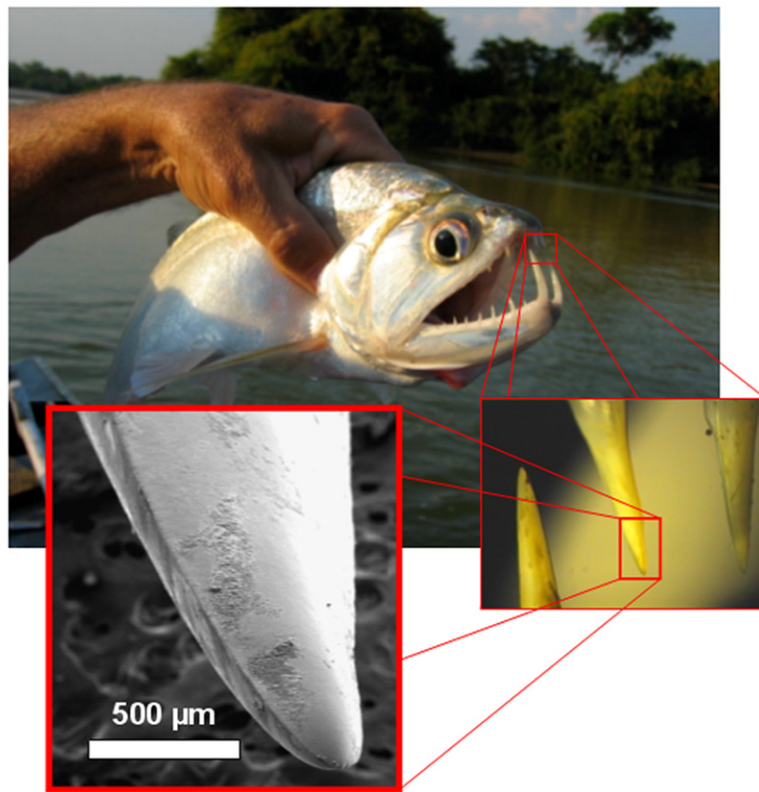


Fig. 19 – Dogfish and teeth. SEM images show the tooth to be sharp and pointed, but not serrated.

is to puncture and hold prey rather than for slicing or sawing prey. Piranha (*Serrasalmus manueli*), on the other hand, has serrated teeth, as shown in the SEM micrographs in Fig. 20(a). There are about 14 teeth on top and 12 on bottom in this fish. The lower teeth are longer and larger than the upper teeth. The jaw is designed with sharp triangular teeth aligned so that as the mouth of the fish closes the initial points of puncture of both the lower and upper jaw are superimposed. As the jaw further closes any tissue caught in the trough of the aligned teeth is severed in a guillotine-like confinement of teeth. This is shown in Fig. 20(b). The large teeth are thin and leaf-like with serrated cutting edge along the entire tooth (Abler, 1992). The periodic distance of the serration is $\sim 25 \mu\text{m}$.

The great white shark has five rows of wedge-shaped, triangular teeth with 26 teeth in both the upper and lower jaws, as shown in Fig. 21(a). These rows of teeth are fluid in the sense that the back teeth migrate to the front as the outermost, primary teeth are broken or torn off. The shark tooth's enamel exhibits a hardness of $\sim 1.5 \text{ GPa}$ while that of its dentine is $\sim 0.25 \text{ GPa}$, approximately 6 times less, similar to the hippo tooth (Fig. 21(b)). These values are lower than those of human teeth, $\sim 4 \text{ GPa}$, and $\sim 0.5 \text{ GPa}$ for enamel and dentine respectively (Imbeni et al., 2003). However, they show a similar relationship in mismatch. The upper teeth are the slicing teeth and have obviously serration, as shown in the SEM micrographs. The serration has a periodic separation distance of $\sim 300 \mu\text{m}$, much larger than in the piranha teeth. The lower teeth are more narrow than the upper teeth and do not have well-defined serrations. The difference is due to functional reasons. The sharp lower teeth, puncturing

teeth are used to pierce the prey, while the upper teeth are used to slice and cut the prey. Because of the serration, the biting force can be concentrated on each point, in comparison with the smooth-edge teeth, and thus have higher cutting efficiency. Other species of shark have differently shaped teeth such as knife-shaped or conical. For example, the sand tiger shark has a reverse curvature on the tip of their teeth, which ensures the initial penetration (Frazzetta, 1988). The inward curvature on the bottom of the lower teeth can hold the prey.

The serration size appears to depend on the diet of the animal. Table 1 lists some carnivorous animals and a piscavore (piranha) with their body mass and serration size. Meat eaters, such as the tyrannosaurid dinosaurs, great white shark and komodo dragon have serration sizes ranging from 300–400 μm , despite having a two order of magnitude difference in body mass, as shown in Table 1. Piranha, normally a fish eater, has a much smaller serration size ($\sim 25 \mu\text{m}$). From this, teeth seem to be optimized for tearing meat (large serrations) or for tearing fish (small serrations).

1.6. Toucan and hornbill beaks

Beaks are composed of ingenious sandwich structures and achieve ultra-lightweight construction. Beaks comprise two components. The face skin, ramphotheca, is made from β -keratin, which maintains certain stiffness mainly for food gathering and functions as a protective barrier from natural environment. The internal foam core made from bone is an extension of bird skull and is usually hollow at the center. The

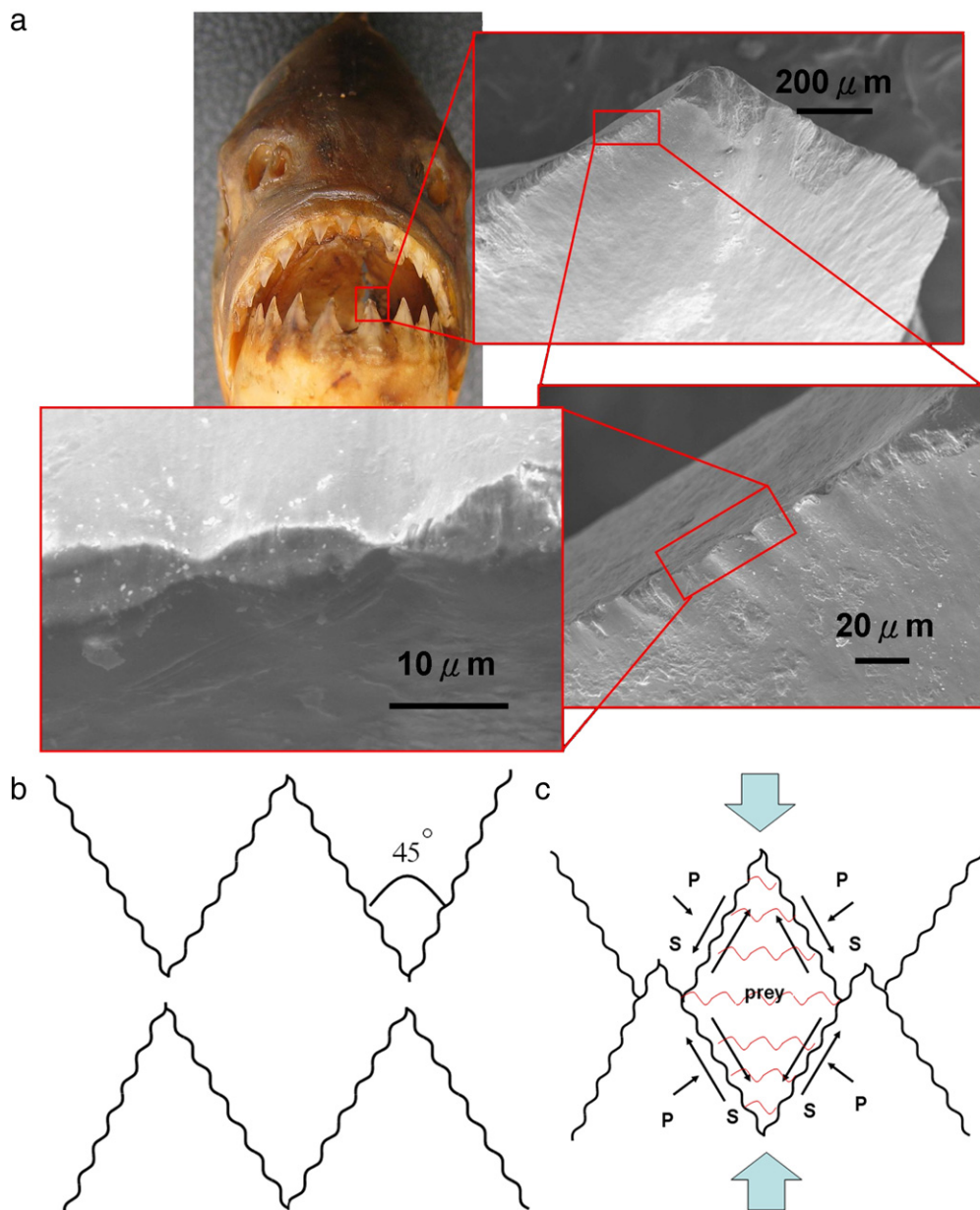


Fig. 20 – Piranha teeth: (a) hierarchical structure from jaw to single tooth to micro serrations; (b) and (c) diagram of guillotine-like confinement of material during the biting action of a piranha.

Table 1 – Teeth serration size and body mass for some carnivorous animals and the piranha

	Serration size (μm)	Body mass (kg)	Reference
Tyrannosauroid dinosaurs	312	6000	Abler (1992)
Great white shark	300	890	This work
Komodo dragon	400	70	Abler (1992)
Piranha	25	1	This work

two components are connected by the dermis. Most beaks usually fall into two categories: short and thick or long and thin. The toucan and hornbill beaks are exceptions – they are both long and thick. The toucan beak is 1/3 of total length of the bird and the hornbill beak is 1/4 of the total length. The unique properties of the Toco toucan (*Ramphastos toco*) and wreathed hornbill (*Aceros undulatus*) beaks motivated a recent study by our group (Seki et al., 2005, 2006) and were investigated in relation to structure and mechanical properties. In previous studies, the mechanical properties of the toucan beak were investigated with analytical models in ambient condition and finite element method is used

toco) and wreathed hornbill (*Aceros undulatus*) beaks motivated a recent study by our group (Seki et al., 2005, 2006) and were investigated in relation to structure and mechanical properties. In previous studies, the mechanical properties of the toucan beak were investigated with analytical models in ambient condition and finite element method is used

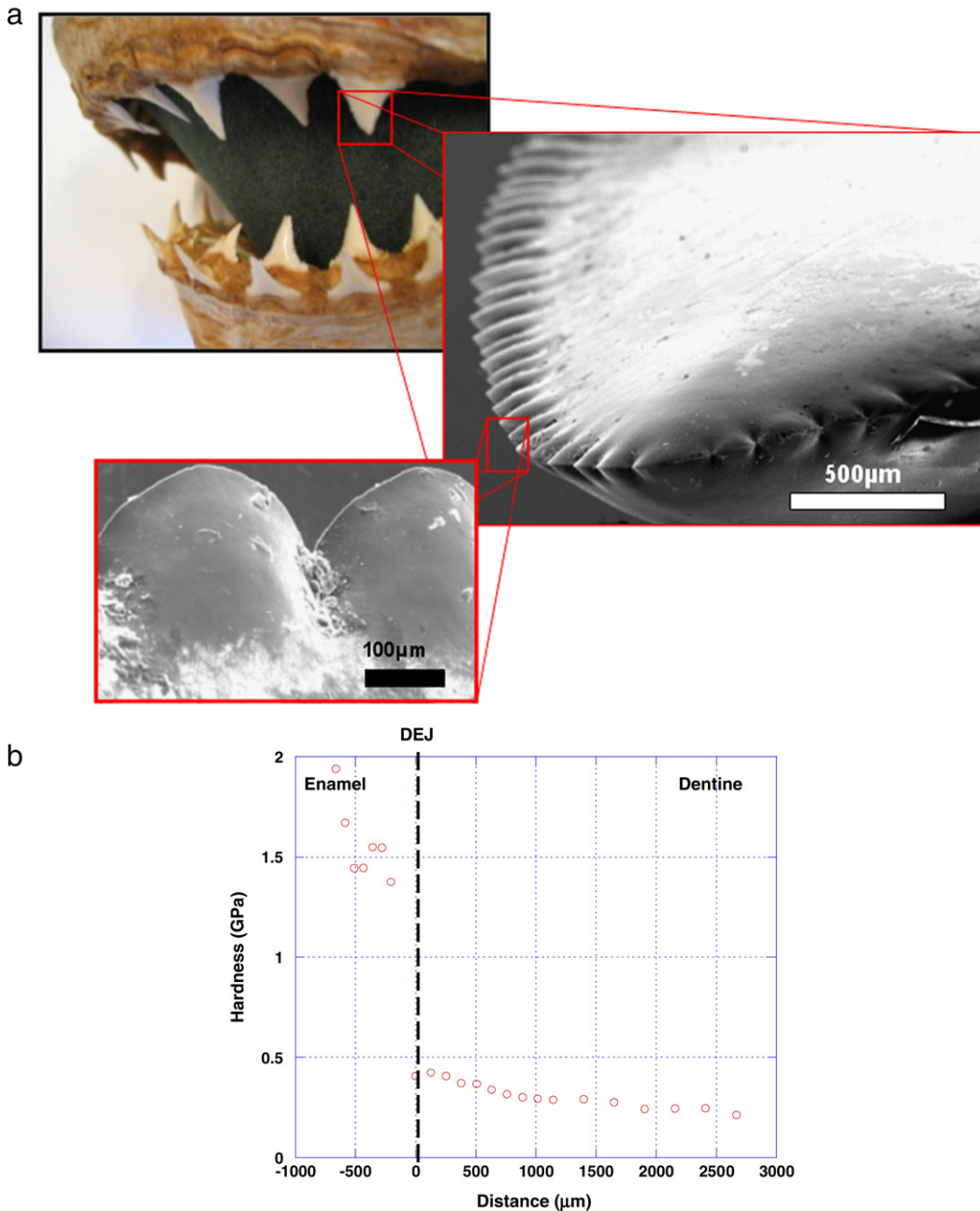


Fig. 21 – Great white shark teeth. (a) SEM images show serration at the edges of the tooth, (b) Hardness test showing the dental/enamel junction.

to model the mechanical responses of beak including the synergistic effect between external shell and foam core (Seki et al., 2005, 2006). In this study, we have further evaluated the structure of beaks with CT scans and the mechanical properties of toucan beak keratin at high humidity condition.

Fig. 22 shows the pictures and SEM micrographs of the toucan and hornbill beak exteriors. Both beak keratins consist of multiple layers of keratin tiles. The toucan ramphotheca surface is constructed from a homogenous distribution of keratin tiles. The diameter of the tile is $\sim 45 \mu\text{m}$ and the thickness of the tile is $\sim 1 \mu\text{m}$. The geometry of tiles is polygonal and symmetric. Three different types of ramphotheca surface are observed in hornbill

exterior keratin. The smooth surface is detected on hornbill ramphotheca and is similar to the toucan ramphotheca surface. The tile has a somewhat elongated shape and aligns in the longitudinal direction. The keratin tile structure on the casque, a projection of the maxillary, is not distinguishable and individual tiles are tightly connected or merged with neighboring tiles. On the ridge surface, the connecting glue is observed in the keratin tile boundary region. The protruded glue differentiates surface morphology from other two surfaces.

The mechanical properties of mammalian keratins are highly influenced by their moisture content (Kitchener and Vincent, 1987; Bertram and Gosline, 1987; Wu et al., 2006).

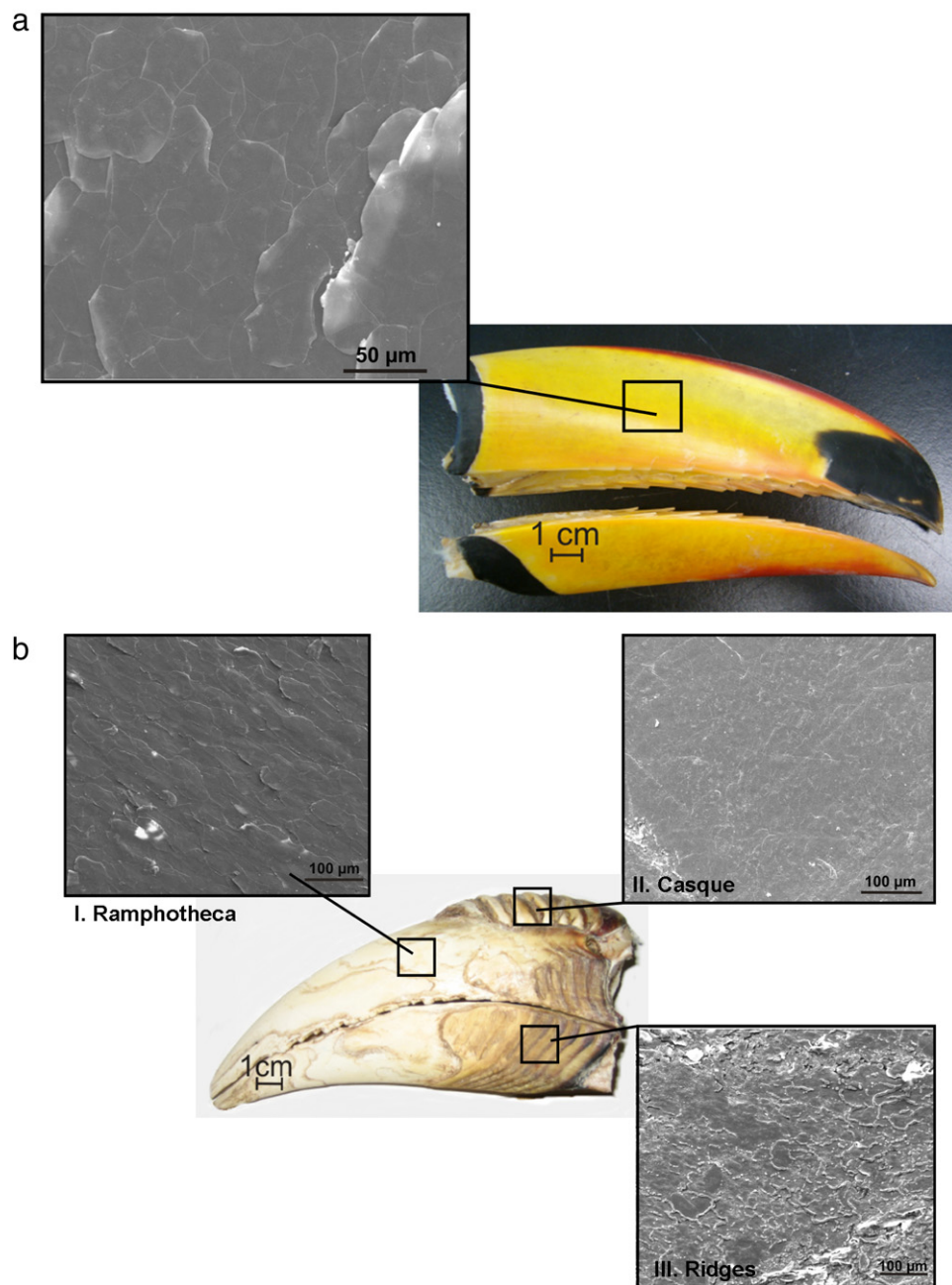


Fig. 22 – SEM micrographs of (a) toucan beak keratin; (b) hornbill beak keratin.

In the case of avian keratins, the stiffness of feathers and claws at high humidity conditions significantly decreases (Taylor et al., 2004). The typical tensile stress-strain curves of toucan beak keratin under two conditions ($23\text{ }^{\circ}\text{C}$ and 45% RH, $38\text{ }^{\circ}\text{C}$ and 95% RH) are shown in Fig. 23. At low humidity, the Young's modulus of toucan keratin is plane isotropic, ranging from $1.04 \pm 0.06\text{ GPa}$ (longitudinal) to $1.12 \pm 0.13\text{ GPa}$ (transverse). The tensile strength of toucan beak keratin in the transverse direction was approximately 32% higher than in longitudinal direction, as shown in Fig. 23(a). The strength of toucan beak keratin significantly decreases under the high humidity condition, as shown in Fig. 23(b). The elongation at 95% RH exhibits approximately two folds

higher than that at 45% RH. The variation in strength in longitudinal and transverse directions is also more distinctive under the high humidity condition. The average strength is $16.7 \pm 2.2\text{ MPa}$ in longitudinal direction and $31.0 \pm 4.4\text{ MPa}$ in transverse direction. The Young's modulus is $0.093 \pm 0.02\text{ GPa}$ (longitudinal) and $0.17 \pm 0.003\text{ GPa}$ (transverse). The stiffness in the high humidity condition drops by approximately an order of magnitude. The mass of hydrated keratin increases $\sim 10\%$ for 5 h of exposure in 95% RH condition, which significantly decreases the mechanical properties of toucan beak keratin.

The toucan and hornbill foam cores consist of closed-cell foam. The purpose of the foam is to have an efficient

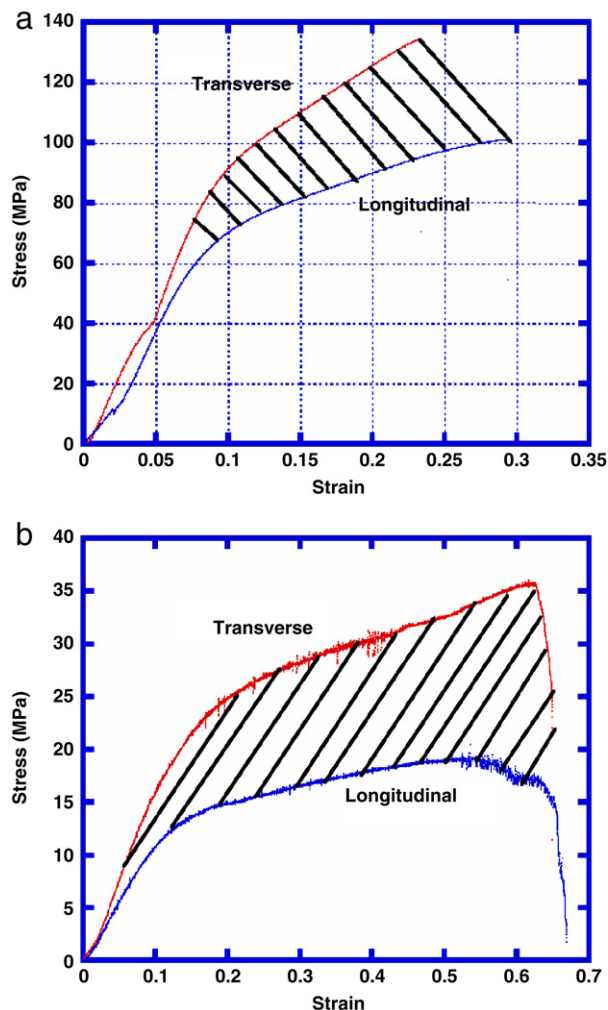


Fig. 23 – Stress-strain curves of toucan beak keratin; (a) 45% RH and 23 °C; (b) 95% RH and 38 °C.

lightweight and high stiffness construction and significant capability for energy absorption. The thin membranes cover individual cells composed of bony rods (trabeculae). The typical cell size of toucan foam is ~ 1 mm and that of hornbill foam is ~ 3 mm. The foam core increases the mechanical stability especially in bending and energy absorption capacity of beak, including the synergism between two components (Seki et al., 2005, 2006). The trabeculae of toucan and hornbill are arranged in complex manner and have high hardness in comparison with beak keratin (Seki et al., 2005, 2006). The microhardness or Vickers hardness of toucan and hornbill keratins is 0.22 ± 0.02 GPa and 0.21 ± 0.07 GPa (smooth surface), respectively, at atmospheric condition. The microhardness of toucan and hornbill foam materials is 0.28 ± 0.04 GPa and 0.39 ± 0.01 GPa. The microhardness of hornbill trabecula is comparable to avian bone (Bonser, 1995). The beak foams collapse in brittle manner and fail by the buckling of rods in compression.

The complex foam interior structure was reconstructed by a 3D visualization technique. We have used 200 image slices from micro-computed tomography at a $93 \mu\text{m}$ of resolution. DDV (Digital Data Viewer) and VTK (Visualization Toolkit)

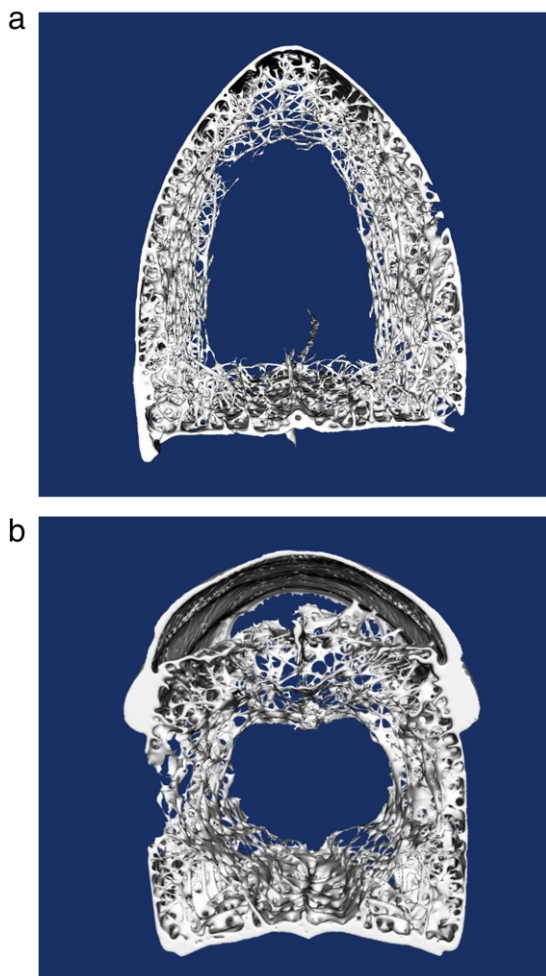


Fig. 24 – Three-dimensional models of beak foams; (a) toucan and (b) hornbill with keratin exterior.

were used to generate isosurface mesh by using marching cube algorithm (Lorensen and Cline, 1987). ImageJ converts the DICOM format of images to tiff format. We took half the size of original image dataset (hornbill; 505×555 , and toucan; 450×505) and doubled the size in visualization process. Fig. 24 shows the 3-dimensional structure of (a) toucan and (b) hornbill foams. 1,373,000 (toucan) and 1,800,000 (hornbill) mesh elements were used to create the contour surface. The exterior of toucan is eliminated and only bony foam is reconstructed. The hornbill foam includes exterior keratin and a secondary hole is observed between bony foam and casque, shown in Fig. 24(b). The models clearly show the hollow structure of foam cores. The beak foams consist of thin-walled structure with an interconnected network of the rods. The membranes disappeared from the models due to the low intensity of the membranes in CT images.

2. Summary

Biological materials are adapted to be multifunctional. At the macroscale, the shape is generally optimized for protection and defense. At the microstructural scale, laminar, porous

and fibrous structures predominate. Mineralized tissues provide protection and/or serve as a weapon and also impart a structural framework. Nacre, antlers, teeth and tusks have a hard, mineralized outer layer and a softer core. In nacre and enamel, the mineralized component is ~95%, far exceeding other mineralized components. The hard outer layer for abalone serves as protection whereas in teeth and tusks, it also provides biting and chewing surfaces. Teeth and tusks also function as defensive and offensive weapons. The shape of teeth is adapted for chewing (flat), piercing (sharp) or biting (sharp) whereas tusks are pointed and serve no function for nutritional purposes. The serrated teeth of predators such as sharks and piranha are additionally adapted to cutting. The softer inner core of teeth (dentin) provides toughness to the tooth with its woven, cross-laminar structure. For the crab exoskeletons, the mineralized portions protect and form a general framework for growth. Antlers, the horseshoe crab exoskeleton and bird beaks contain a porous substance in the core. For antlers, it primarily provides stiffness and energy absorbance. For bird beaks it serves as a lightweight framework and also functions for energy absorption.

3. Material sources

Abalone was harvested from the abalone tank located at the Scripps Institute of Oceanography. Sheep crabs were obtained locally from a fish market. A horseshoe crab was collected on a beach in Long Island, NY. Antlers and tusks were purchased from Into the Wilderness Trading Company, Pinedale, WY. The Curator of Birds at the San Diego Zoo's Wild Animal Park kindly provided us with hornbill beaks. Mr. Jerry Jennings, owner of Emerald Forest Bird Gardens, provided the toucan beaks. Teeth were obtained from piranha and the Amazon dogfish caught in Brazil. Great white shark teeth were provided by Scripps Institute of Oceanography from their collection. Rat teeth were from a field rat.

Acknowledgements

We gratefully acknowledge support from Professor Falko Kuester for the 3-D visualization, Jacqueline Corbeil for the computer tomography scans, Evelyn York for scanning electron microscopy, Paul Price and Damen Toroian for demineralizing the antler and Moopi for chasing down the rat. This research was funded by the National Science Foundation, Division of Materials Research, Biomaterials Program (Grant DMR 0510138).

REFERENCES

- Abler, W.L., 1992. The serrated teeth of tyrannosaurid dinosaurs, and biting structures in other animals. *Paleobiol.* 18 (2), 161–183.
- Ashby, M.F., 1989. On the engineering properties of materials. *Acta Metall.* 37 (5), 1273–1293.
- Addadi, L., Joester, D., Nudelman, F., Weiner, S., 2006. Mollusk shell formation: A source of new concepts for understanding biominerization process. *Chem. Eur. J.* 12, 980–987.
- Arzt, E., Gorb, S., Spolenak, R., 2003. From micro to nano contacts in biological attachment devices. *Proc. Natl. Acad. Sci. USA* 100, 10603–10606.
- Autumn, K., Liang, Y.A., Hsieh, S.T., Zesch, W., Chan, W.P., Kenny, T.W., Fearing, R., Full, R.J., 2000. Adhesive force of a single gecko foot-hair. *Nature* 405, 681–685.
- Barthelat, F., Li, C.M., Comi, C., Espinosa, H.D., 2006. Mechanical properties of nacre constituents and their impact on mechanical performance. *J. Mater. Res.* 21, 1977–1986.
- Bertram, J.E.A., Gosline, J.M., 1987. Functional design of horse hoof keratin: The modulation of mechanical properties through hydration effects. *J. Exp. Biol.* 130, 121–136.
- Bevelander, G., Nakahara, H., 1970. An electron microscope study of the formation and structure of the periostracum of a gastropod. *Littorina littorea*. *Calc. Tiss. Res.* 5, 1–12.
- Blob, R.W., LaBarbera, M., 2001. Correlates of variation in deer antler stiffness: Age, mineral content, intra-antler location, habitat and phylogeny. *Biol. J. Linn. Soc.* 74, 113–120.
- Blob, R.W., Snelgrove, J.M., 2006. Antler stiffness in moose (*Alces alces*): Correlated evolution of bone function and material properties? *J. Morph.* 267, 1075–1086.
- Bonser, R.H.C., 1995. Longitudinal variation in mechanical competence of bone along the avian humerus. *J. Exp. Biol.* 198, 209–212.
- Bouligand, Y., 1972. Twisted fibrous arrangements in biological materials and cholesteric meso phases. *Tissue Cell* 4, 189–217.
- Cartwright, J.H.E., Checa, A.G., 2007. The dynamics of nacre self-assembly. *J. R. Soc. Inter.* 4, 491–504.
- Chapman, D.I., 1975. Antlers—bones of contention. *Mamm. Rev.* 5 (4), 121–172.
- Chen, P.Y., Lin, A.Y.M., McKittrick, J.M., Meyers, M.A., 2008. Structure and mechanical properties of crab exoskeletons. *Acta Biomater.* in press (doi:10.1016/j.actbio.2007.12.010).
- Clutton-Brock, T.H., 1982. The function of antlers. *Behaviour* 79, 108–124.
- Craig, R.G., Peyton, F.A., Johnson, D.W., 1961. Compressive properties of enamel, dental cements and gold. *J. Dent. Res.* 40, 936–945.
- Craig, R.G., Peyton, F.A., 1958. Elastic and mechanical properties of human dentin. 37, 710–718.
- Currey, J.D., 1979. Mechanical properties of bone tissues with greatly differing functions. *J. Biomech.* 12, 313–319.
- Currey, J.D., 1988. The effect of porosity and mineral content on the Young's modulus of elasticity of compact bone. *J. Biomech.* 21, 131–139.
- Currey, J.D., 1989. Strain rate dependence of the mechanical properties of reindeer antler and the cumulative damage model of bone fracture. *J. Biomech.* 22, 469–475.
- Currey, J.D., 1990. Physical characteristics affecting the tensile failure properties of compact bone. *J. Biomech.* 23, 837–844.
- Erben, H.K., 1972. On the structure and growth of the nacreous tablets in gastropods. *Biominer.* 7, 14–27.
- Espinosa, E.O., Mann, M.J., 1991. Identification guide for ivory and ivory substitutes. US Fish and Wildlife Services, Forensics Laboratory, Ashland, Oregon.
- Falini, G., Albeck, G.S., Weiner, S., Addadi, L., 1996. Control of aragonite or calcite polymorphism by mollusk shell macromolecules. *Science* 271, 67–69.
- Feng, Q.L., Li, H.B., Cui, F.Z., Li, H.D., 1999. Crystal orientation domains found in the single lamina in nacre of the *Mytilus edulis* shell. *J. Mater. Sci. Lett.* 18, 1547–1549.
- Frazzetta, T.H., 1988. The Mechanics of cutting and the form of shark teeth (Chondrichthyes, Elasmobranchii). *Zoomorphology* 108, 93–107.
- Fritz, M., Belcher, A.M., Radmacher, M., Walters, D.A., Hansma, P.K., Stucky, G.D., Morse, D.E., Mann, S., 1994. Flat pearls from biofabrication of organized composites on inorganic substrates. *Nature* 371, 49–51.

- Gao, H.J., Ji, B.H., Jäger, I.L., Arzt, E., Fratzl, P., 2003. Materials become insensitive to flaws at nanoscale: Lessons from nature. *Proc. Natl. Acad. Sci. USA* 100, 5597–5600.
- Geist, V., 1966. The evolution of horn-like organs. *Behaviour* 27, 175–214.
- Giraud-Guillem, M.M., 1984. Fine structure of the chitin-protein system in the crab cuticle. *Tissue Cell* 16, 75–92.
- Goss, R.J., 1983. Deer Antlers: Regeneration, Function and Evolution. Academic Press, New York.
- Harvey, P.H., Bradbury, J.W., 1991. Sexual selection. In: Krebs, J.R., Davies, N.B. (Eds.), *Behavioural Ecology: An Evolutionary Approach*. Blackwell Scientific, Oxford, pp. 203–233.
- Henshaw, J., 1971. Antlers—the unbrittle bones of contention. *Nature* 231, 469.
- Imbeni, V., Nalla, R.K., Bosi, C., 2003. In vitro fracture toughness of human dentin. *J. Biomed. Mater. Res. A* 66, 1–9.
- Imbeni, V., Nalla, R.K., Marshall, G.W., Marshall, S.J., Ritchie, R.O., 2005. The dentin-enamel junction and the fracture of human teeth. *Nature Mater.* 4, 229–232.
- Jackson, A.P., Vincent, J.F.V., Turner, R.M., 1988a. The mechanical design of nacre. *Proc. Royal Soc. Lond. B* 234, 415–440.
- Jackson, A.P., Vincent, J.F.V., Turner, R.M., 1988b. Comparison of nacre and other ceramic composites. *Proc. Royal Soc. Lond. B* 234, 415.
- Ji, B.H., Gao, H.J., 2004. Mechanical properties of nanostructure of biological materials. *J. Mech. Phys. Solid* 52, 1963–1990.
- Kitchener, A., Vincent, J.F.V., 1987. Composite theory and the effect of water on the stiffness of horn. *J. Mater. Sci.* 22, 1385–1389.
- Laws, R.M., 1968. Dentition and aging of the hippopotamus. *East African Wildlife Journal* 6, 19–52.
- Lin, A.Y.M., Meyers, M.A., 2005. Growth and structure in abalone shell. *Mater. Sci. Eng. A* 290, 27–41.
- Lin, A.Y.M., Meyers, M.A., Vecchio, K.S., 2006. Mechanical properties and structure of *Strombus gigas*, *Tridacna gigas* and *Haliothis rufescens* sea shells: A comparative study. *Mater. Sci. Eng. C* 26, 1380–1389.
- Lin, A.Y.M., Chen, P.Y., Meyers, M.A., 2007. The growth of nacre in the abalone shell. *Acta Biomater.* 4, 131–138.
- Lincoln, G.A., 1972. The role of antlers in the behavior of red deer. *J. Exp. Zool.* 182, 233–249.
- Lorensen, W.E., Cline, H.E., 1987. Marching cubes: A high resolution 3D surface construction algorithm. *Comput. Graph.* 21, 163–169.
- Manne, S., Zaremba, C.M., Giles, R., Huggins, L., Walters, D.A., Belcher, A.M., Morse, D.E., Stucky, G.D., Didymus, J.M., Mann, S., Hansma, P.K., 1994. Atomic force microscopy of the nacreous layer in mollusc shells. *Proc. Royal Soc. B.* 236, 17–23.
- Marshall, G.W., Marshall, S.J., Kinney, J.H., Balooch, M., 1997. The dentin substrate: Structure and properties related to bonding. *J. Dent.* 25, 441–458.
- Meister, W., 1956. Changes in biological structure of the long bones of white-tailed deer during the growth of antlers. *Anat. Rec.* 124, 709–721.
- Menig, R., Meyers, M.H., Meyers, M.A., Vecchio, K.S., 2000. Quasi-static and dynamic mechanical response of *Haliothis rufescens* (abalone) shells. *Acta. Mater.* 48, 2383–2398.
- Meyers, M.A., Chen, P.Y., Lin, A.Y.M., Seki, Y., 2008a. Biological materials: Structure and mechanical properties. *Progr. Mater. Sci.* 53, 1–206.
- Meyers, M.A., Lin, A.Y.M., Chen, P.Y., Muyco, J., 2008b. Mechanical strength of abalone nacre: Role of the soft organic layer. *J. Mech. Behav. Biomed. Mater.* 1, 76–85.
- Muir, P.D., Sykes, A.R., Barrell, G.K., 1987. Calcium metabolism in red deer (*Cervus elaphus*) offered herbages during antlerogenesis: kinetic and stable balance studies. *J. Agric. Sci. Camb.* 109, 357–364.
- Nakahara, H., Bevelander, G., Kakei, M., 1982. Electron microscopic and amino acid studies on the outer and inner shell layers of *Haliothis rufescens*. *Venus Jpn. J. Malac.* 41, 33–46.
- Nalla, R.K., Kinney, J.H., Ritchie, R.O., 2003. Effect of orientation on the in vitro fracture toughness of dentin: The role of toughening mechanisms. *Biomaterials* 24, 3955–3968.
- Raabe, D., Sachs, C., Romano, P., 2005. The crustacean exoskeleton as an example of a structurally and mechanically graded biological nanocomposite material. *Acta. Mater.* 53, 4281–4292.
- Rajaram, A., Ramanathan, N., 1982. Tensile properties of antler bone. *Calc. Tiss. Int.* 34, 301–305.
- Sarikaya, M., Aksay, I.A., 1992. Nacre of abalone shell: A natural multifunctional nanolaminated ceramic-polymer composite material. In: Case, S.T. (Ed.), *Results and Problems in Cell Differentiation —Biopolymers*. Springer-Verlag, Berlin, pp. 1–26.
- Schäffer, T.E., Zanetti, C.I., Proksch, R., Fritz, M., Walters, D.A., Almqvist, N., Zaremba, C.M., Morse, D.E., Hansma, P.K., 1997. Does abalone nacre form by heteroepitaxial nucleation or by growth through mineral bridges? *Chem. Mater.* 9, 1731–1740.
- Seki, Y., Schneider, M.S., Meyers, M.A., 2005. Structure and mechanical properties of the toucan beak. *Acta. Mater.* 53, 5281–5296.
- Seki, Y., Kad, B., Benson, D., Meyers, M.A., 2006. The toucan beak: Structure and mechanical response. *Mater. Sci. Eng. C* 26, 1412–1420.
- Snodgrass, S.M., Gilbert, P.W., 1967. A shark bite meter. In: Gilbert, P.W., Mathewson, R.F., Rall, D.P. (Eds.), *Sharks, Skates and Rays*. The Johns Hopkins University Press, Baltimore, pp. 331–337.
- Song, F., Zhang, X.H., Bai, Y.L., 2002. Microstructure and characteristics in the organic matrix layers of nacre. *J. Mater. Res.* 17, 1567–1570.
- Srinivasan, A.V., Haritos, G.K., Hedberg, F.L., 1991. Biomimetics: Advancing man-made materials through guidance from nature. *Appl. Mech. Rev.* 44, 463–482.
- Taylor, A.M., Bonser, R.H.C., Farrent, J.W., 2004. The influence of hydration on the tensile and compressive properties of avian keratinous tissues. *J. Mater. Sci.* 39, 939–942.
- Towe, K.M., Hamilton, G.H., 1968. Ultrastructure and inferred calcification of the mature and developing nacre in bivalve mollusks. *Calc. Tiss. Res.* 1, 306–318.
- van der Lang, N.J., van Dijk, A.J.M., Dortmans, L.H.M.G., de With, G., 2002. Fracture toughness of calcium hydroxyapatite and spinel at different humidities and loading rates. *Key Eng. Mater.* 206–213, 1599–1602.
- Vincent, J.F.V., 1991. Structure Biomaterials. Princeton University Press, New Jersey.
- Vincent, J.F.V., 2002. Arthropod cuticle: A natural composite shell system. *Composites A* 33, 1311–1315.
- Vollrath, F., Madsen, B., Shao, Z., 2001. The effect of spinning conditions on the mechanics of a spider's dragline silk. *Proc. Royal Soc. B* 268, 2339–2346.
- Wada, K., 1964. Studies on the mineralization of calcified tissues in molluscs – VIII. Behavior of eosinophil granules and of organic crystals in the process of mineralization of secreted organic matrices in glass coverslip preparations. *Nat. Pearl Res. Lab.* 9, 1087–1098.
- Watanabe, N., Wilber, K.M., 1960. Influence of the organic matrix on crystal type in mollusks. *Nature* 188, 334.
- Wegst, U.G.K., Ashby, M.F., 2004. The mechanical efficiency of natural materials. *Philos. Mag.* 84, 2167–2186.
- Wu, K.S., van Osdol, W.W., Dauskardt, R.H., 2006. Mechanical properties of human stratum corneum: Effects of temperature, hydration, and chemical treatment. *Biomaterials* 27, 785–795.
- Zaremba, C.M., Belcher, A.M., Fritz, M., Li, Y., Mann, S., Hansma, P.K., Morse, D.E., Stucky, G.D., 1996. Critical transitions in the biofabrication of abalone shells and flat pearls. *Chem. Mater.* 8, 679–690.